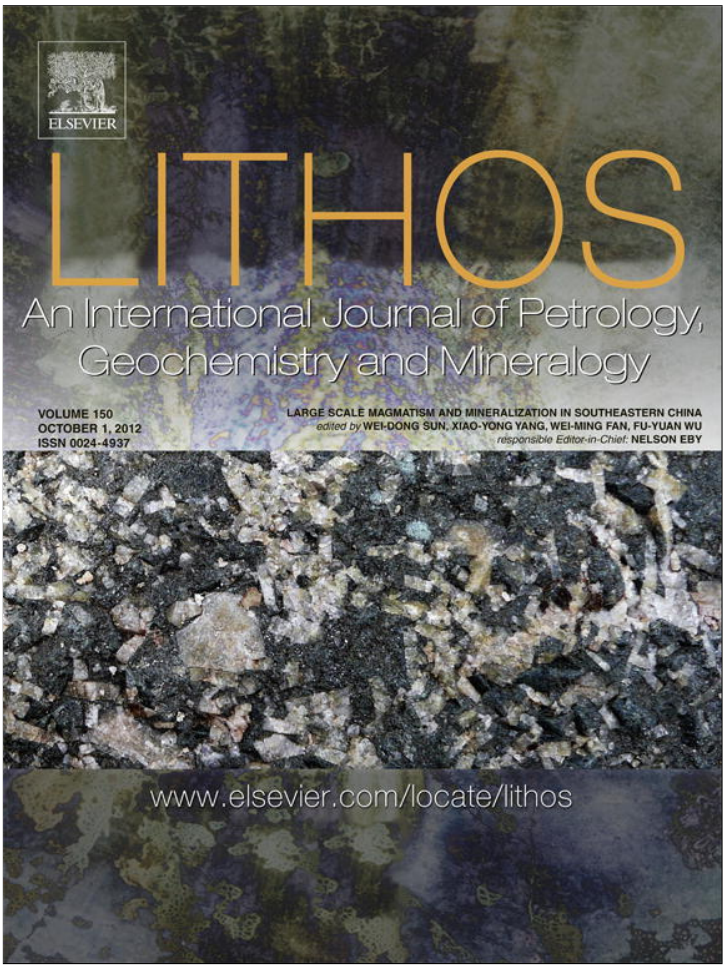

Lithos 150 (2012) 85–100

Contents lists available at SciVerse ScienceDirect

Lithos

journal homepage: www.elsevier.com/locate/lithos

Remelting of Neoproterozoic relict volcanic arcs in the Middle Jurassic: Implication for the formation of the Dexing porphyry copper deposit, Southeastern China

Xuan Liu [a], Hong-Rui Fan [a,*], M. Santosh [b], Fang-Fang Hu [a], Kui-Feng Yang [a], Qiu-Li Li [c], Yue-Heng Yang [c], Yongsheng Liu [d]

[a] Key Laboratory of Mineral Resources, Institute of Geology and Geophysics, Chinese Academy of Sciences, Beijing 100029, China
[b] Division of Interdisciplinary Science, Faculty of Science, Kochi University, Kochi 780-8520, Japan
[c] State Key Laboratory of Lithospheric Evolution, Institute of Geology and Geophysics, Chinese Academy of Sciences, Beijing 100029, China
[d] State Key Laboratory of Geological Processes and Mineral Resources, China University of Geosciences, Wuhan 430074, China

ARTICLE INFO

Article history:
Received 13 September 2011
Accepted 18 May 2012
Available online 28 May 2012

Keywords:
Island arc
Geochronology
Geochemistry
Zircon Hf–O isotopes
Dexing Cu deposit
Southeastern China

ABSTRACT

The Dexing copper deposit in southeastern China is a typical non-arc porphyry deposit, the origin of which has been a topic of debate for several decades. Here we present new results from U–Pb geochronology, whole-rock chemistry and Sr–Nd–Hf–O isotopic investigations on the ore-forming granodioritic porphyry. LA-ICPMS zircon U–Pb data suggest that the granodioritic porphyry was formed in the Middle Jurassic (ca. 172.5 Ma) probably associated with lithospheric thinning driven by either sub-continental lithospheric mantle delamination or asthenospheric upwelling. The porphyry displays both arc-like and adakitic trace element signatures. The adakitic features suggest that HREE (heavy rare earth elements)-rich minerals such as garnet and hornblende, in the absence of plagioclase resided in the source region. The arc-like signatures are broadly comparable with those of the proximal Neoproterozoic island arc rocks including the keratophyre from Shuangxiwu Group and associated granitoids indicating a potential genetic relationship. The porphyry has chondritic $\varepsilon Nd(t)$ of −0.28 to 0.25 and radiogenic $\varepsilon Hf(t)$ of 2 to 7, and correspondingly, uniform two stage depleted mantle Nd model ages of 940–980 Ma and Hf model ages of 800–1100 Ma (mean ~920 Ma). On Nd and Hf isotopic evolution diagrams, these values are markedly similar to those of the adjacent Neoproterozoic arc rocks when calculated forward to the Mid-Jurassic. Zircons of the porphyry show mantle-like oxygen isotope characters with $\delta^{18}O$ values clustering in the range of 4.7–5.9‰, similar to the values for the Neoproterozoic arc rocks mentioned above. The geochemical and isotopic features recorded in our study suggest mantle-derived magmas with no significant supracrustal input for the source of the porphyry. With regard to the source of the Cu ore, we consider a model involving the remelting of sulfide-bearing arc-related lower crustal source. Furthermore, the occurrence of a Neoproterozoic VMS (volcanic massive sulfide) type copper deposit (the Pingshui Cu deposit) in the Shuangxiwu Group might suggest that the lower crustal rocks related to a Neoproterozoic relict island arc provided the source for copper during a second stage melting event. We propose a new geodynamic model for the Dexing porphyry Cu deposit which envisages that the sulfide-bearing arc lower crustal rocks were generated during oceanic slab subduction in the early Neoproterozoic, the remnants of which were preserved at the crust/mantle boundary. Subsequently, in the Middle Jurassic, these rocks were heated by asthenospheric upwelling and remelted to produce fertile magmas. The magmas ascended along the Northeast Jiangxi Fault and intruded into the Jiuling terrane where Cu precipitation occurred upon subsequent magma cooling and fluid exsolution.

1. Introduction

Porphyry copper deposits are the most important suppliers of Cu resources around the world. They are commonly associated with intermediate-acid porphyritic intrusions in volcanic arcs generated by partial melting of metasomatized asthenospheric mantle overriding a subducting oceanic lithosphere (Richards, 2003, 2011). Recent studies have led to the discovery of a number of copper deposits which occur in non-arc settings (Hou and Yang, 2009, Hou et al., 2001, 2003, 2004, 2006a, 2006b, 2007, Hou et al., 2011; Richards, 2009, 2011; Yang and Hou, 2009). However, in spite of the contrast in tectonic settings, these deposits share many characters with arc-related porphyry copper deposits, suggesting a genetic link. Thus, Richards (2009) termed these deposits as "post-subduction porphyry copper deposits", and proposed that the ore-forming magmas were produced by partial melting of subduction modified upper plate lithosphere, during which process

* Corresponding author. Tel.: +86 10 82998218; fax: +86 10 62010846.
E-mail address: fanhr@mail.igcas.ac.cn (H-R. Fan).

0024-4937/$ – see front matter © 2012 Elsevier B.V. All rights reserved.
doi:10.1016/j.lithos.2012.05.018

the ore-forming fluids and metallic components (such H_2O, Cu, etc.) were remobilized from the remnants of the previous arc magmas (Richards, 2011 and references therein). In a recent overview on non-arc porphyry copper deposits in the eastern Tethyan metallogenic belt of China, Hou et al. (2011) noted that the ore-forming magmas are typically high potassic calc-alkaline, and show geochemical affinity with adakitic rocks. They, therefore, suggested that the magmas were derived through the partial melting of a thickened mafic lower crust or delaminated lower crust, with juvenile mantle inputs which provided the source of Cu.

The Dexing Cu deposit in the southeastern China is a giant porphyry type ore deposit, hosting ~8.5 Mt Cu, ~0.3 Mt Mo and ~20 t Au (Li and Sasaki, 2007; Rui et al., 1984). The ore deposit formed in the Middle Jurassic as inferred from the Re–Os molybdenite age of ~170 Ma (Mao and Wang, 2000; Zhou et al., 2011). Although previous studies suggested that the ore deposit was formed in a volcanic arc setting related to the subduction of paleo-Pacific ocean (Sun et al., 2010; Zhou et al., 2011; Zhu et al., 1983), there are several lines of evidence which suggest that the Dexing Cu deposit was formed in a non-arc (intracontinental) setting (Hou et al., 2011, and references therein; Wang et al., 2004, 2006, and references therein). The latest subduction event recognized in this region was terminated some 800 m.y. before the ore formation (Charvet et al., 1996; Chen et al., 1991). In this respect, it is different from typical arc porphyry Cu deposits. However, deposit-scale features similar to arc porphyry copper deposits, including close relationship with intrusions, hydrothermal alteration types and zoning, ore mineral occurrence and assemblages, have been recorded from Dexing deposit, and the ore-forming porphyry displays arc-like geochemical signatures. These seem to indicate potential influence of arc-derived materials on the ore formation. Some earlier studies suggested that the ore-forming granodioritic porphyry originated from depleted mantle or through mixing between mantle and crustal materials, based on preliminary Sr–Nd isotopic studies (Qian and Lu, 2005; Zhu et al., 1983, 1990, 2002). With the advancement of research on the adakitic rocks in various parts of China and the discovery of adakitic signatures in Dexing granodioritic porphyry, revised models were proposed where the rock was considered to be a product of the partial melting of delaminated lower crust and subsequent equilibration of the melts with the lithospheric mantle (Wang et al., 2004, 2006) or by partial melting of a thickened mafic crust which was infiltrated by asthenospheric mantle "batches" (Hou et al., 2011). These and several other explanations are, to some extent, incompetent for both magma and ore genesis.

In this study, we present geochemical, isotopic and geochronological data from the granodiorite porphyry at Dexing and compare our results with those from the Neoproterozoic arc rocks nearby. We propose a new model which envisages the formation of the Cu deposit through remelting of lower crust carrying the relics of a Neoproterozoic island arc.

2. Geological background

South China consists of Yangtze block in the north and Cathaysia block in the south, separated by a Meso- to Neoproterozoic orogen which is commonly referred to as "Jiangnan Orogen" (Li et al., 2009; Wu et al., 2006; Ye et al., 2007; Zheng et al., 2008). The Jiangshan-Shaoxing Fault (JSF) is believed to be the suture zone between Yangtze and Cathaysia (Fig. 1a). The orogen is composed of pre-Sinian rocks, interpreted as the basement of the Yangtze Block (1.85–0.8 Ga), and a cover sequence of Sinian (0.8–0.57 Ga) and post-Sinian sedimentary strata of neritic and terrestrial facies (Wang, 1986). The pre-Sinian rocks are Mesoproterozoic to Neoproterozoic clastic sediments and associated volcanic rocks, which, from SW to NE, comprise the Sibao Group in northern Yunnan province, Banxi Group in northern Yunnan and western Hunan provinces, Lengjiaxi Group in eastern Hunan province, Shuangqiaoshan Group in northern Jiangxi province, Shangxi Group in southern Anhui province and Shuangxiwu Group in northwestern Zhejiang province (Shen et al., 1993). The Shuangxiwu Group was formed in the early Neoproterozoic (Li et al., 2009), and the other Groups were formed predominantly in the Mesoproterozoic.

The eastern part of Jiangnan Orogen, where Dexing porphyry Cu deposit is located, covers a large area of southern Anhui, northwestern Zhejiang and northeastern Jiangxi provinces (Fig. 1b). It is subdivided

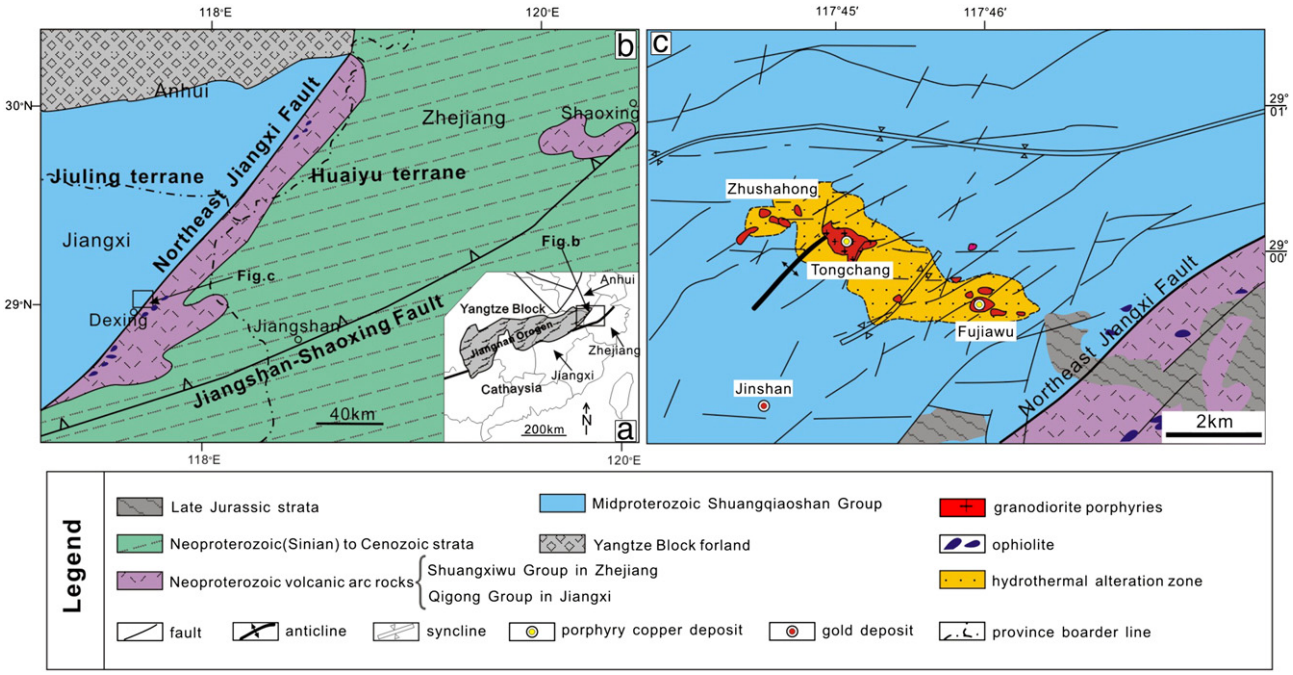

Fig. 1. Geological maps of the Jiangnan Orogen and the Dexing porphyry copper deposit.
Panel a is adapted from Wu et al. (2006); panel b is adapted from Guo et al. (1996); panel c is adapted from Zhu et al. (1983).

into Jiuling and Huaiyu terranes along Northeast Jiangxi Fault (NEJF) (Charvet et al., 1996; Lin et al., 1993; Shi et al., 1994).

The Jiuling terrane is a strongly deformed, EW-trending anticlinorium. In surface exposure, the eastern flank of the terrane structurally underlies the Qigong Group of the Huanyu terrane. Aeromagnetic traverses across the contact at one locality, however, suggest that the contact may actually be overturned. The majority of the exposed area consists of slate, tuff, phyllite and locally meta-basalt belonging to the Shuangqiaoshan and Shangxi Groups. Locally, the Mesoproterozoic rocks are uncomformably overlain by Neoproterozoic conglomerate. Only a small area of these strata is preserved (Shi et al., 1994). These strata are intruded by small bodies of granodiorite, plagiogranite, and biotite granite, which were dated at ~820 Ma (SHRIMP on zircons, Li et al., 2001). Locally, the Proterozoic strata are overlain by upper Paleozoic and late Jurassic strata, which are devoid of deformation.

The Huaiyu terrane contains remnants of a Neoproterozoic continental arc (Charvet et al., 1996; Guo et al., 1996), which is represented by the Shuangxiwu Group in northwestern Zhejiang and Qigong Group in northeastern Jiangxi. The Shuangxiwu Group was divided into four formations according to lithologic characteristics, including the Pingshui, Beiwu, Yanshan and Zhangcun Formation (Li et al., 2009). The Pingshui Formation predominantly consists of altered basaltic to andesitic rocks. Keratophyres from this formation were dated at ~905 Ma by Chen et al. (2009). The Taohong and Xiqiu granitoids intruding into the Pingshui Formation were arc-derived magmatic rocks formed at ~910 Ma (Ye et al., 2007). The Beiwu Formation consists of andesite, dacite and rhyolite as well as volcaniclastic interbeds, and it is conformably overlain by Yanshan Formation which mainly consists of felsic tuff, tuffaceous sandstones and siltstones. The Zhangcun Formation consists chiefly of felsic ignimbrite dated at ~890 Ma (Li et al., 2009). Qigong Group mainly distributes along the NEJF. It consists of an extremely disrupted sequence of turbidities and volcaniclastic and spilite–keratophyre in this group were dated at 1113 ± 53 Ma by Sm–Nd isochron method, with an $\varepsilon_{Nd}(t)$ value of 7.4 and model ages of 1088–1172 Ma (Lin et al., 1993). A suite of ophiolitic rocks (the Zhangshudun ophiolite), which is dated at ~1.0 Ga by Sm–Nd isochron method (Chen et al., 1991) and 968 ± 23 Ma by SIMS zircon U–Pb (Li et al., 1994), occurs within the Qigong Group.

The Cu mineralization at the Dexing Cu deposit is closely related to a Middle Jurassic granodioritic porphyry intruded into the phyllite and slate of the Shuangqiaoshan Group of Jiuling terrane (Wang et al., 2004, 2006; Zhu et al., 1983). The porphyry system consists of three individual plutons: the Zhushahong in the northwest, Tongchang in the middle, and Fujiawu in the southeast with surface exposures of 0.06, 0.7 and 0.6 km^2 respectively (Fig. 1c). They were coevally emplaced at 171–172 Ma (Zhou et al., 2011). Three discrete cap-like alteration-mineralization systems were also developed centered on each pluton. In each system, both granodioritic porphyry and wallrocks suffered different types of hydrothermal alteration. According to alteration mineral assemblages and their distribution in the systems, Zhu et al. (1983) recognized several concentric zones which include potassic (biotite–K-feldspar–chlorite–illite) in the innermost part, propylitic (chlorite–hydromuscovite or chlorite dominated) in outer areas separated by phyllic, and phyllic alteration (sericite–quartz) developed in the contact zone between the intrusion and metamorphic wall rocks. Zhu et al. (1983) further pointed out that these zones distribute symmetrically along the intrusion/wallrock contact in addition to a concentric distribution pattern. It should be noted that the potassic and propylitic assemblages are slightly different from what were originally defined by Lowell and Guilbert (1970) in that they may have been overprinted by later fluids as evidenced by the occurrence of illite and/or chlorite in the assemblages. The ores predominantly occur as both sulfide veins and disseminated sulfides in the phyllic zone. It was estimated by Zhu et al. (1983) that over two thirds of the ores were hosted in the phyllic zone.

3. Petrography

Giant porphyry Cu systems often have a prolonged magmatic history, accompanied by several stages of intrusive events, with the Cu mineralization generally associated with the latest events (Sillitoe, 2010). However, at the Dexing porphyry Cu deposit, only a single intrusive event (granodioritic porphyry) has been recognized within each pluton, with only minor late granitic aplite and quartz dioritic porphyry dispersing nearby (Zhu et al., 1983). The fresh grayish granodiorite shows porphyritic texture and massive structure. Phenocrysts accounting for up to 60 vol.% of the rocks comprise subhedral–euhedral plagioclase (mainly andesine, Zhu et al., 1983), hornblende, biotite, K-feldspar and minor quartz. The matrix is composed of crystalline plagioclase, quartz, K-feldspar and minor amount of hornblende and biotite. Accessory minerals include magnetite, apatite, titanite, ilmenite and zircon. The phenocrystic plagioclase is typically large in size (0.2–1 cm) and accounts for 40–60 vol.% of the phenocryst phases. The feldspar commonly displays albite or Carlsbad twins, and some of them show distinct compositional zoning. The minerals in the porphyry samples that we examined show varying degrees of hydrothermal alteration, especially the matrix and mafic minerals.

4. Analytical methods

Five representative samples of the granodioritic porphyry (09D45, 09D52, 09D64, 09D107 and 09D122) from the Tongchang pluton were selected in this study for a combined LA-ICPMS zircon U–Pb geochronology and in situ Lu–Hf isotopic analyses. Among these, three samples (09D45, 09D52 and 09D64) were also chosen for SIMS zircon O isotopic analyses. The whole rock element analyses were performed on eight granodioritic porphyry samples from the Zhushahong (09D01, 09D02) and Tongchang (09D52, 09D68, 09D72, 09D78, 09D82 and 09D83) plutons, among which five samples (09D01, 09D52, 09D68, 09D78 and 09D82) were also analyzed for Sm–Nd isotopes.

4.1. Zircon selection and imaging

After crushing, the whole-rock samples were processed by conventional magnetic and density techniques to separate zircons, followed by hand-picking under a binocular microscope. Selected zircons were mounted in epoxy and polished. The grains were first imaged under reflected and transmitted light by optical microscope, and then by cathodoluminescence (CL) in a LEO1450 scanning electronic microscope at the Institute of Geology and Geophysics, Chinese Academy of Sciences (IGGCAS). The obtained photographs were used as a guide in selection of spots for U–Pb dating.

4.2. Whole-rock major, trace elements and Sr–Nd isotopes

Whole rock samples for element and isotopic analyses were ground into powders of ~200 mesh in size. For major element analysis, 0.5 g powders were accurately weighed and then ignited under 1000 °C for about 60 min. The weight loss divided by original weight (0.5 g) is taken as "LOI (Loss On Ignition)" as listed in Table 2. The ignited powders were then mixed with powders of 67 wt.% $Li_2B_4O_7$ + 33 wt.% $LiBO_2$ (5 g), and melted to make glass pellets. The pellets were then analyzed by X-ray fluorescence spectroscopy (XRF) with an AXIOS Minerals spectrometer at the IGGCAS. The analytical uncertainties were basically within 0.1–1% (RSD).

Trace element abundances were obtained by inductively coupled plasma mass spectrometry (ICP-MS) using a Finnigan MAT Element spectrometer, with analytical uncertainties within 5% for most elements, at the IGGCAS. Whole rock powders (40 mg) were dissolved in distilled $HF + HNO_3$ in 15 ml high-pressure Teflon bombs at 200 °C

for 5 days, dried and then diluted to 50 ml for analysis. A blank solution was analyzed and the total procedural blank was <50 ng for all trace elements. Indium was used as an internal standard to correct for matrix effects and instrument drift. Precision for all trace elements is estimated to be 5% and accuracy is better than 5% for most elements by analyses of the GSR-1 standard.

Strontium and Nd isotopic compositions were measured by thermal ionization mass spectrometry (TIMS) using a Finnigan MAT 262 system at the IGGCAS, following the procedure described by Lan et al. (2011). Procedural blanks were <100 pg for Sm and Nd, and <300 pg for Rb and Sr. The isotopic ratios were corrected for mass fractionation by normalizing to $^{86}Sr/^{88}Sr = 0.1194$ and $^{146}Nd/^{144}Nd = 0.7219$, respectively. The measured values for the JNdi-1 Nd standard and NBS987 Sr standard were $^{143}Nd/^{144}Nd = 0.512118 \pm 12$ (2σ, n = 10) and $^{87}Sr/^{86}Sr = 0.710257 \pm 12$ (2σ, n = 10), respectively. USGS reference material BCR-2 was measured to monitor the accuracy of the analytical procedures, with the following results: $^{143}Nd/^{144}Nd = 0.512633 \pm 13$ (2σ, n = 12) and $^{87}Sr/^{86}Sr = 0.705035 \pm 12$ (2σ, n = 12).

4.3. Zircon U–Pb dating and in situ Hf isotopic analyses

U–Pb dating of zircons was conducted by LA-ICPMS at the State Key Laboratory of Geological Processes and Mineral Resources, China University of Geosciences, Wuhan. Detailed operating conditions for the laser ablation system and the ICP-MS instrument and data reduction are the same as those described by Liu et al. (2008, 2010a,b). Laser sampling was performed using a GeoLas 2005. An Agilent 7500a ICP-MS instrument was used to acquire ion-signal intensities. Helium was applied as a carrier gas. Argon was used as the make-up gas and mixed with the carrier gas via a T-connector before entering the ICP. Nitrogen was added into the central gas flow (Ar + He) of the Ar plasma to decrease the detection limit and improve precision. Each analysis incorporated a background acquisition of approximately 20–30 s (gas blank) followed by 50 s data acquisition from the sample. The Agilent Chemstation was utilized for the acquisition of each individual analysis. Off-line selection and integration of background and analytical signals, and time-drift correction and quantitative calibration for U–Pb dating were performed by ICPMSDataCal (Liu et al., 2008, 2010a). Zircon 91500 was used as external standard for U–Pb dating, and was analyzed twice every 5 analyses. Time-dependent drifts of U–Th–Pb isotopic ratios were corrected using a linear interpolation (with time) for every five analyses according to the variations of 91500 (i.e., 2 zircon 91500 + 5 samples + 2 zircon 91500). Preferred U–Th–Pb isotopic ratios used for 91500 are from Wiedenbeck et al. (1995). Uncertainty of preferred values for the external standard 91500 was propagated to the ultimate results of the samples. Concordia diagrams and weighted mean calculations were made using Isoplot/Ex_ver3 (Ludwig, 2003).

In situ zircon Hf isotopic analyses were conducted on the same spots where U–Pb dating was performed on a Neptune MC-ICPMS equipped with a Geolas-193 laser-ablation microprobe at the IGGCAS. A stationary spot was used for the present analyses, with a beam diameter of 63 μm (predominantly) or 31.5 μm. Zircon 91500 was used as the reference standard afterwards, with a recommended $^{176}Hf/^{177}Hf$ ratio of 0.282306 ± 10 (Woodhead et al., 2004). All the Hf isotope analysis results were reported with the error in 2σ of the mean. A decay constant of 1.865×10^{-11} year^{-1} for ^{176}Lu (Scherer et al., 2001) was adopted. Initial $^{176}Hf/^{177}Hf$ ratios $\varepsilon_{Hf}(t)$ were calculated with reference to the chondritic reservoir (CHUR) of Blichert-Toft and Albarède (1997) at the time of zircon growth from the magma. Single-stage Hf model age (T_{DM1}) is calculated relative to the depleted mantle with present-day $^{176}Hf/^{177}Hf = 0.28325$ and $^{176}Lu/^{177}Hf = 0.0384$ (Griffin et al., 2000). Instrumental conditions and data acquisition were described in detail by Xu et al. (2004) and Zheng et al. (2008).

4.4. In situ SIMS zircon O isotopic analyses

In situ zircon oxygen isotope analyses were measured using Cameca IMS 1280 SIMS at the IGGCAS, with analytical procedures that were similar to those reported by Li et al. (2010b). The Cs^+ primary ion beam was accelerated at 10 kV, with an intensity of ca. 2 nA (Gaussian mode with a primary beam aperture of 200 μm to reduce aberrations) and rastered over a 10 μm area. The spot is about 20 μm in diameter (10 μm beam diameter + 10 μm raster). The normal-incidence electron flood gun was used to compensate for sample charging during analysis with homogeneous electron density over a 100 μm oval area. Negative secondary ions were extracted with a 10 kV potential. The field aperture was set to 5000 μm, and the transfer-optics magnification was adjusted to give a field view of 125 μm (FA = 8000). Energy slit width was 30 eV, the mechanical position of the energy slit was controlled before starting the analysis (5 eV gap, −500 digits with respect to the maximum). The entrance slit width is ~120 μm and exit slit width for multicollector Faraday cups (FCs) for ^{16}O and ^{18}O is 500 μm (MRP = 2500). The intensity of 16O was typically 1 × 109 cps. Oxygen isotopes were measured in multi-collector mode using two off-axis Faraday cups. The NMR (Nuclear Magnetic Resonance) probe was used for magnetic field control with stability better than 2.5 ppm over 16 h on mass 17. One analysis takes ~4 min consisting of pre-sputtering (~120 s), automatic beam centering (~60 s) and integration of oxygen isotopes (10 cycles × 4 s, total 40 s). Uncertainties on individual analyses are reported at 1σ level. With low noise on the two FC amplifiers, the internal precision of a single analysis is generally better than 0.2‰ for $^{18}O/^{16}O$ ratio. Values of $\delta^{18}O$ are standardized to VSMOW and reported in standard per mil notation. The instrumental mass fractionation factor (IMF) is corrected using 91500 zircon standard with $\delta^{18}O_{VSMOW} = 9.9‰$ (Wiedenbeck et al., 2004). Measured $^{18}O/^{16}O$ is normalized by using Vienna Standard Mean Ocean Water compositions (VSMOW), then corrected for the instrumental mass fractionation factor (IMF) as follows: $(\delta^{18}O)_M = (((^{18}O/^{16}O)_M/0.0020052) - 1) \times 1000(‰)$; $IMF = (\delta^{18}O)_{M,standard} - (\delta^{18}O)_{VSMOW}$; $\delta^{18}O_{Sample} = (\delta^{18}O)_M + IMF$.

5. Results

5.1. Geochronology

The timing of formation of the Dexing granodioritic porphyry has been the subject of investigation since the 1980s (Jin et al., 2002; Wang et al., 2004; Zhou et al., 2011; Zhu et al., 1983, 1990, 2002). The earlier dates obtained by bulk rock Rb–Sr or Sm–Nd isochrons show a wide spread (165–184 Ma) and have large errors (Jin et al., 2002; Zhu et al., 1983, 1990, 2002) resulting from the disturbance of the isotopic systems by hydrothermal alteration. Wang et al. (2004) reported an age of 171 ± 3 Ma using SHRIMP zircon U–Pb dating and interpreted it as the emplacement age of the Dexing granodioritic porphyry. Zhou et al. (2011) obtained an age of ~171 Ma by LA-ICPMS zircon U–Pb dating. In order to further constrain the timing of magma emplacement, we conducted LA-ICPMS zircon U–Pb dating of the Dexing granodioritic porphyry.

Zircons from our samples are transparent, colorless and large (the long axes of the largest grains are up to 500 μm). They have prismatic dipyramidal, euhedral crystal shapes and exhibit clear oscillatory zoning in cathodoluminescence (CL) images (Fig. 2), suggesting their magmatic crystallization history. None of the zircons with an exception of 09D107 #7 contains an inherited core which is identifiable by its brightness under CL (Fig. 2d). Several zircons have uneven rims (09D107 #13, 09D122 #6, #12, #21; Fig. 2d,e), which show bright CL and have “abnormal” ages as seen below.

5.1.1. Sample 09D45

Twenty one spots were analyzed in zircons from this sample (Supplemental Electronic Data Table 1). On a U–Pb concordia diagram,

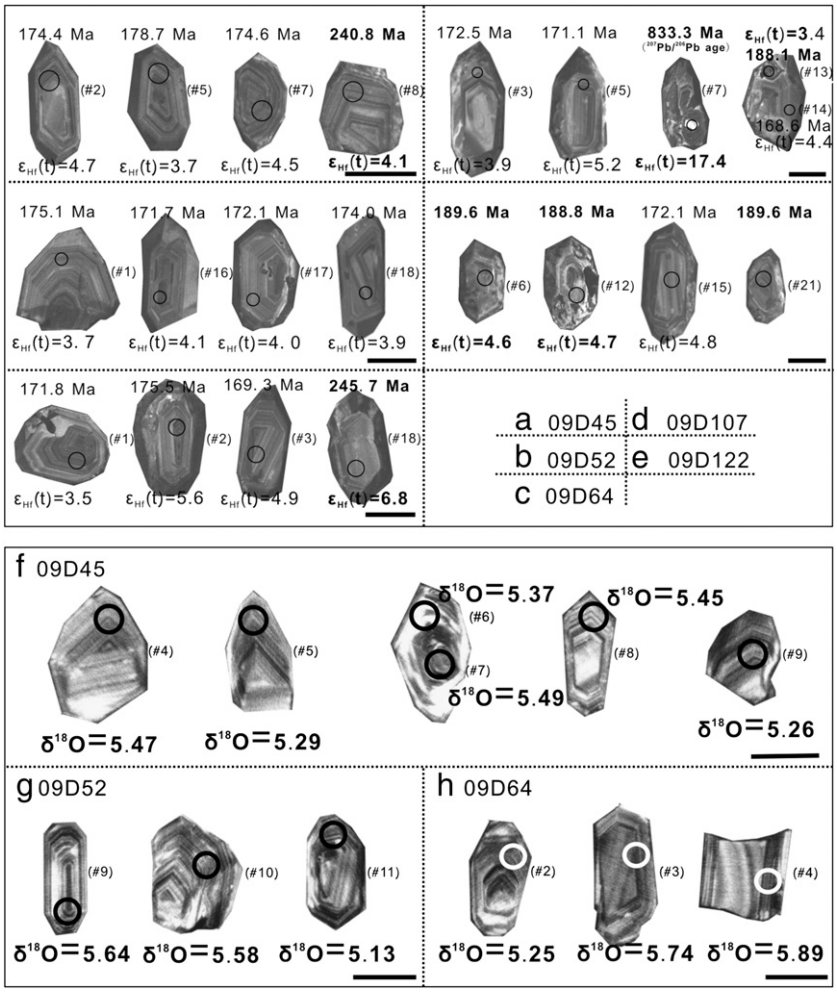

Fig. 2. Cathodoluminescence images of zircons from the granodioritic porphyry at the Dexing porphyry copper deposit. Circles in a–e indicate the analytical spots for LA-ICPMS U–Pb dating and LA-MC-ICPMS Hf isotopic analysis. Circles in f–h indicate the analytical spots for SIMS oxygen isotopic analysis, the results of which are denoted as "$\delta^{18}O$" values (‰). Numbers in the parentheses indicate the spot number of analysis. All the scales are 100 μm.

all the data points plot on or close to the concordia, with twenty spots being tightly clustered and yielding a weighted mean $^{206}Pb/^{238}U$ age of 173.8 ± 1.3 Ma (1σ) (Fig. 3a). We interpret this age to represent the timing of crystallization of zircons in sample 09D45. The remaining age (spot #8, Fig. 2a) is concordant ($^{206}Pb/^{238}U$ age = 240.8 ± 2.4 Ma) and significantly larger that the others. Triassic igneous activities were documented from Lingshan granite (~234 Ma, K–Ar on biotite, Zhu et al., 1983) in this area. Therefore, this zircon might reflect contamination from these sources.

5.1.2. Sample 09D52

Twenty two spots were analyzed for this sample (Supplemental Electronic Data Table 1). On a U–Pb concordia diagram, all the data points plot close to or on concordia, yielding a weighted mean $^{206}Pb/^{238}U$ age of 173.2 ± 0.8 Ma (1σ) (Fig. 3b).

5.1.3. Sample 09D64

Twenty seven spots were analyzed on zircons from this sample (Supplemental Electronic Data Table 1). On a U–Pb concordia diagram (Fig. 3c), twenty five data points show close cluster, yielding a weighted mean $^{206}Pb/^{238}U$ age of 171.4 ± 1.0 Ma (1σ) which is interpreted as the crystallization age for this sample. The data from spot #11, although concordant, yielded a $^{206}Pb/^{238}U$ age about 10 Ma younger than that of the others, and was therefore not included in the mean $^{206}Pb/^{238}U$ age calculation. Spot #18 yielded a $^{206}Pb/^{238}U$ age of 246 Ma, and similar to spot #8 in 09D45, the age might suggest inheritance from adjacent Triassic granite.

5.1.4. Sample 09D107

Twenty spots were analyzed on zircons from this sample (Supplemental Electronic Data Table 1). On a U–Pb concordia diagram (Fig. 3d), a discordia line is defined by two discordant data (spots #7 and #13) and the other eighteen concordant data points, with an upper intercept at ~946 Ma and lower intercept at ~170 Ma. Spot #7 represents the inherited core, yielding a $^{206}Pb/^{238}U$ age of 478 Ma, $^{207}Pb/^{235}U$ age of 543 Ma and $^{207}Pb/^{206}Pb$ age of 833 ± 96 Ma. The $^{207}Pb/^{206}Pb$ age is considered to be close to the crystallization age since the $^{207}Pb/^{206}Pb$ ratio is insensitive to Pb loss (Faure, 1977). The upper intercept is interpreted as the best estimate of the crystallization age. Spot #13 hits a cavity (Fig. 2d) and an analysis on the same grain yielded a $^{206}Pb/^{238}U$ age of ~169 Ma (spot #14, Fig. 2d). The analysis of spot #13 was likely to reflect hydrothermal alteration effect. The eighteen concordant data points yielded a weighted mean $^{206}Pb/^{238}U$ age of 171.9 ± 1.0 Ma (1σ) which is interpreted to represent the crystallization age of the sample. Although only one Proterozoic zircon was observed, it might represent inheritance from an older source region and suggest that the source rocks were likely formed in the early Neoproterozoic.

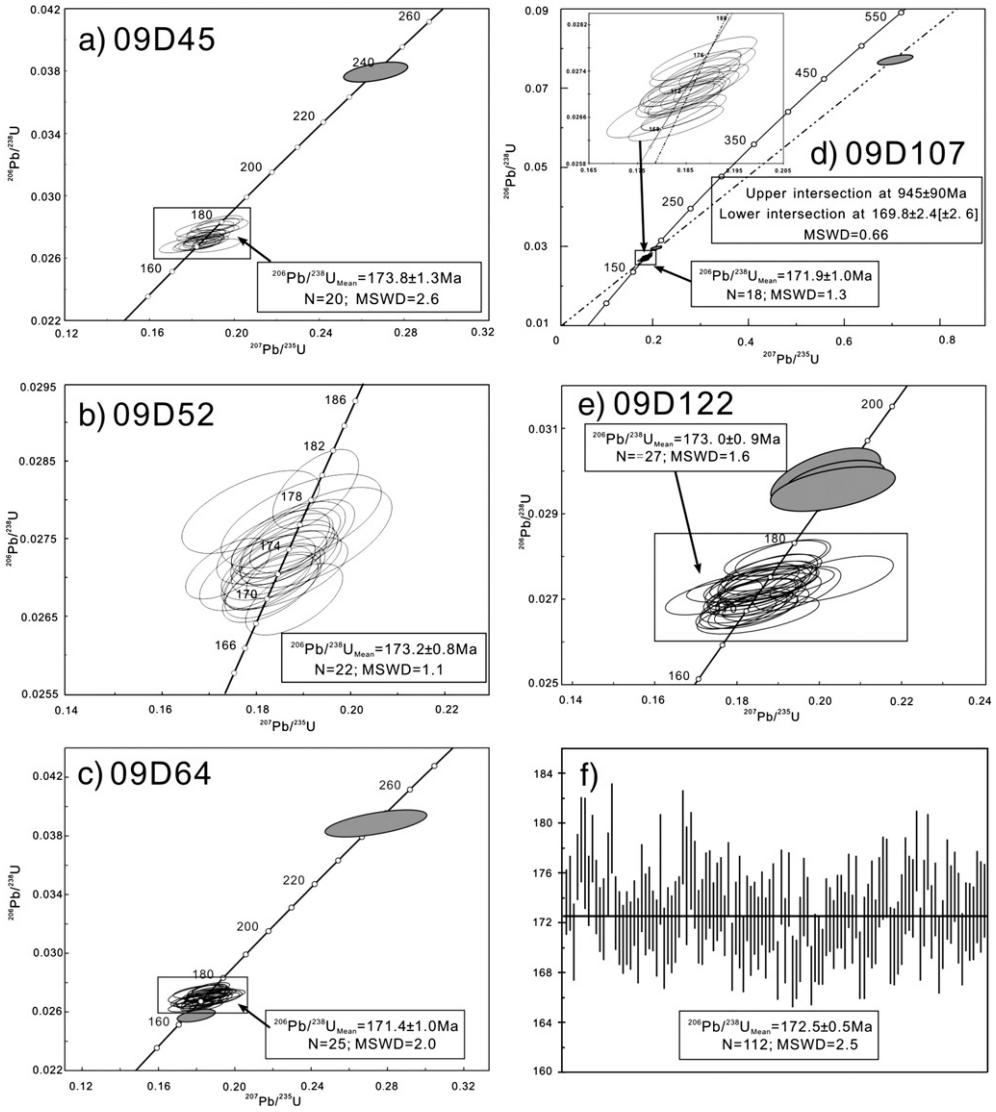

Fig. 3. U–Pb concordia diagrams constructed from zircon U–Pb isotopic compositions of granodioritic porphyry at the Dexing porphyry copper deposit. Solid gray ellipses denote the data points excluded from mean $^{207}Pb/^{206}Pb$ age calculations. Panel f shows a weighted average calculation of all concordant data points.

5.1.5. Sample 09D122

Thirty spots were analyzed on zircons from this sample (Supplemental Electronic Data Table 1). On a U–Pb concordia diagram (Fig. 3e), all the data points plot on a concordia. Twenty seven spots show close cluster, yielding a weighted mean $^{206}Pb/^{238}U$ age of 173.0 ± 0.9 Ma (1σ). The remaining three zircons yielded ~190 Ma, and they, as mentioned earlier, show bright rims or surfaces, which might reflect hydrothermal modification. Therefore, these "abnormal" analyses are interpreted to be resulted from U loss or Pb gain by hydrothermal alteration.

In summary, the zircons from five representative rock samples analyzed by LA-ICPMS in our study yielded weighted mean $^{206}Pb/^{238}U$ ages of 173.8 ± 1.3 Ma, 173.2 ± 0.8 Ma, 171.4 ± 1.0 Ma, 171.9 ± 1.0 Ma and 173.0 ± 0.9 Ma. Because these dates overlap within 2σ, we obtain an age of 172.5 ± 0.5 Ma (N = 112, MSWD = 2.5; Fig. 3f) by calculating a weighted average of all concordant data points.

5.2. Major/trace elements and element mobility

A summary of the petrological observations of the selected samples for elemental and isotopic analyses under a polarization microscope is presented in Table 1, and the analytical results of major and trace elements are listed in Table 2.

Any suite of rocks which has been subjected to hydrothermal alteration or metamorphism is likely to suffer element mobility (Rollinson, 1993). It is therefore essential in any trace element study to demonstrate first that element concentrations are undisturbed and the original information is preserved before any inferences can be made about the petrogenesis. Element mobility might have been an essential feature of the porphyry samples that we used for geochemical analyses in this study as a result of the extensive hydrothermal alteration observed in this ore deposit. Previous geochemical studies had also faced this issue (Rui et al., 1984; Wang et al., 2004, 2006; Zhou et al., 2011; Zhu et al., 1983). In this section, we discuss the validity of applying the results from geochemical study based on a combination of the data from petrological observations, and the analytical results and associated investigations conducted by other workers.

The analyzed samples show varying degrees of mineralogical alteration (Table 1), and correspondingly, their LOI values are relatively large, ranging from 1.72 to 4.27%. In general, major elements except for Ti, Fe, Al, are mobile during hydrothermal alteration (Sturchio et al., 1986). All the samples from our study show uniform TiO_2 (0.42–0.48 wt.%) and Al_2O_3 (13.99–15.94 wt.%) concentrations, and these results are similar to those in previous works from this area (Rui et al., 1984; Wang et al., 2004, 2006; Zhou et al., 2011; Zhu et al., 1983). It can therefore be safely assumed that Ti and Al were

Table 1
Petrological observation results for samples used for elemental and isotopic analyses.

Sample no.	Sampling location	Detailed description
09D02	Zhushahong	Most plagioclase phenocrysts were completely replaced by clay minerals, carbonates and minor muscovite; most biotite phenocrysts were completely replaced by muscovite, carbonates, clay minerals and pyrites; matrix were altered into muscovite, secondary quartz and minor clay minerals
09D52	Tongchang	Most plagioclase phenocrysts stayed unaltered, and the remaining were partially replaced by sericite; minor biotite phenocrysts were subject to replacement by carbonates and chlorites; matrix remained nearly unchanged with only minor silicification
09D68	Tongchang	Plagioclases in both phenocrysts and matrix were completely replaced by sericite; biotite phenocrysts were altered into chlorites; matrix suffered fairly strong silicification
09D72	Tongchang	Biotite and hornblende phenocrysts were replaced by secondary biotites; plagioclase phenocrysts suffered very slight replacement by sericite; matrix subjected minor silicification
09D78	Tongchang	A small amount of plagioclase phenocrysts was partially altered into sericite; a small number of biotite phenocrysts were replaced by secondary quartz, chlorites and hematite along cleavage planes; matrix was partially replaced by biotites, secondary quartz, hematite and minor chlorites
09D82	Tongchang	Most plagioclase phenocrysts were altered into sericite or muscovite; most biotite phenocrysts suffered replacement by chlorites, carbonates and minor hematite; matrix was replaced by muscovite, secondary quartz and minor sericite
09D83	Tongchang	Most plagioclase phenocrysts remained unchanged, with only minor replacement by sericite; a small number of biotite phenocrysts were replaced by chlorites, hematite; matrix suffered very slight silicification

Note: Sample 09D01 was too small to satisfy thin section making after sample preparation for geochemical analysis, thus description of its petrological characteristics was impossible.

not affected by the alteration. Si is generally regarded as mobile during hydrothermal alteration. But the solubility of SiO_2 is practically negligible when compared to high content of SiO_2 in granitic rocks, and thus Si is considered conservative (Pandarinath et al., 2008). In the present samples, the SiO_2 contents are relatively uniform, varying from 60.58 to 66.37 wt.%, and we therefore neglect the alteration effects on Si. $Fe_2O_3^t$ concentrations show a wide variation from 3.26 to 9.61 wt.% and petrological observations show secondary hematite replacement after biotite suggesting a marked influence on Fe during the hydrothermal alteration. Na, K, Ca, Mg are easily mobilized by hydrothermal fluids (Kelepertsis and Esson, 1987; McHenry, 2009; Sturchio et al., 1986). Extensive alteration of plagioclase is noticed in most samples except for 09D52 and 09D83 (Table 1), and this is directly reflected in the significant variation in Na_2O concentrations (0.01–3.44 wt.%). In addition, other minerals such as K-feldspar, hornblende, biotite also show common alteration in all the analyzed samples (Table 1). We thus consider that K, Ca and Mg were affected by hydrothermal alteration and have hence been not included in petrogenetic interpretations.

Among trace elements, the large ion lithophile elements (LILE, including Cs, Sr, Rb, and Ba) are readily mobilized by hydrothermal fluids, whereas the high field strength elements (HFSE, including Hf, Ti, Nb, Ta, P, and REE (rare earth elements)) are immobile (Humphris and Thompson, 1978; Rollinson, 1993; Sturchio et al., 1986), although some workers have demonstrated that REE, Zr, Ti are also mobile (Pandarinath et al., 2008; references therein) particularly in CO_2-rich fluids (Humphries, 1984) and saline-alkaline fluids (McHenry, 2009). In our trace element data, the Rb contents are relatively uniform (89.94–136.09 ppm) and are similar to the published results with small LOIs (Wang et al., 2006; Zhou et al., 2011), suggesting only limited effect from alteration. Sr and Ba concentrations show significant variations: 171.7 to 1145.3 ppm and 995.3 to 1943.5 ppm, and we only use the data in a later section for a comparative purpose. Although some workers consider that saline-CO_2 fluids were active at the Dexing porphyry Cu deposit (Jin, 1999; Liu et al., 2011; Pan et al., 2009; Qian et al., 2003; Zhu et al., 1983; Zuo et al., 2007), the REE and the other HFSE seem to be unaffected by these fluids. Therefore, we mainly employ the concentrations of Si, Rb, Sr, Ba, REE, and HFSE for petrogenetic interpretations in a later section.

Previous workers have discussed the chemical characteristics of the Dexing granodioritic porphyry (Rui et al., 1984; Wang et al., 2004, 2006; Zhou et al., 2011; Zhu et al., 1983). Most of these studies suggested that the Dexing granodioritic porphyry shows typical calc-alkaline signature. Wang et al. (2004, 2006) demonstrated that the porphyry has an adakitic affinity with high Sr content and La/Yb and Sr/Y ratios, and low Y and Yb content.

The results from our study corroborate the published data, although element mobility considerations alert that the inferences drawn from the concentrations and ratios of some elements in previous studies should be viewed with caution. As demonstrated above, the Dexing granodioritic porphyry has SiO_2 contents of 60.58–66.37%, TiO_2 contents of 0.42–0.57%, and Al_2O_3 contents of 13.99–15.94%. On a Zr/TiO_2 vs. SiO_2 diagram (Fig. 4), most of the data points plot within the calc-alkaline, rhyodacite–dacite field, with the exception of two data points which plot in the andesite field.

The bulk REE contents in our samples range from 66.01 to 196.91 ppm, with a strong fractionation between light and heavy REE ($(La/Lu)_N$ ratios range from 16 to 28) and in the absence of marked Eu anomalies ($(Eu/Eu^*)_N = 0.84–1$). On a chondrite-normalized REE distribution diagram (Fig. 5a), the Dexing granodioritic porphyry exhibits a LREE-enriched, HREE-depleted pattern and lacks Eu anomalies. These features are broadly similar to that of the keratophyre from the Shuangxiwu Group and Taohong–Xiqiu granitoids, with the Dexing granodioritic porphyry showing a slightly higher enrichment in LREE and depletion in HREE.

The Dexing granodioritic porphyry possesses typical arc-like trace element signatures. On the primitive mantle normalized "spider" diagram (Fig. 5b), enrichment in LILE (Rb, Ba, Sr), LREE, Th and U, depletion in HFSE (Nb, Ta, Zr, Hf, Ti), and pronounced negative anomalies of Nb, Ta, Ti positive anomalies of Sr, Ba, Pb anomalies are observed. Samples 09D01 and 09D02 show some exception in that they have negative Sr, Ba anomalies probably resulting from the hydrothermal alteration as discussed in a previous section.

It is also important to note that the Dexing granodioritic porphyry has geochemical features similar to those of the adakitic rocks described by Defant and Drummond (1990). But our results, Sr contents in particular, do not permit us to make discussions toward this direction. Fortunately, this aspect was discussed in detail by Wang et al. (2006). We will briefly review this issue in more detail in a later section.

5.3. Sr–Nd isotopes

The results of whole rock Sr and Nd isotope analyses are listed in Table 2. The initial $^{87}Sr/^{86}Sr$ ratios show significant variation from 0.7050 to 0.7070, indicating a marked disturbance of the Rb–Sr isotopic system. Therefore, Sr ratios are not included for further discussion. Nd isotopic ratios are more resistant to hydrothermal alteration as compared with Sr. Our results show that the Dexing granodioritic porphyry has uniform $\varepsilon_{Nd}(t)$ values ranging from −0.28 to 0.25, with two-stage depleted mantle model ages ($T_{DM,2}$) of 940–980 Ma, which are generally in consistence with the results of previous

Table 2
Results of whole-rock major, trace element analysis and Sr, Nd isotopic analysis.

Sample	09D001	09D002	09D052	09D068	09D072	09D078	09D082	09D083	Keratophyre	Granitoids	Volcanic rocks
	Zhushahong				Tongchang				Shuangxiwu Group From Chen et al. (2009)	Xiqiu and Taohong From Ye et al. (2007)	Shuangxiwu Group From Li et al. (2009)
Major elements (%)											
SiO_2	66.37	64.58	60.58	63.88	65.35	62.70	63.52	65.21	62.50–65.68	56.72–69.03	
TiO_2	0.48	0.42	0.57	0.46	0.42	0.46	0.47	0.47	0.40–0.84	0.32–0.68	
Al_2O_3	15.39	15.92	15.49	15.94	14.30	13.99	14.76	15.36	14.51–15.35	13.80–16.99	
FeOt	1.14	2.12	3.78	2.52	2.58	3.91	3.14	2.67			
Fe_2O_3t	3.26	4.25	6.24	4.92	7.46	9.61	6.67	5.69	4.76–7.93	4.46–8.37	
MnO	0.02	0.06	0.02	0.03	0.02	0.02	0.05	0.03	0.07–0.11	0.06–0.19	
MgO	2.37	2.26	3.80	2.41	2.32	2.78	2.55	2.75	2.00–2.70	1.69–3.68	
CaO	3.27	3.08	3.02	2.77	2.11	2.64	3.25	2.57	2.00–4.51	1.98–8.47	
Na_2O	0.01	1.95	3.44	2.53	2.45	2.69	1.79	3.17	3.09–4.31	2.84–4.32	
K_2O	4.06	3.06	2.20	2.62	3.56	2.19	2.92	2.74	0.74–1.82	0.6–2.83	
P_2O_5	0.31	0.27	0.30	0.27	0.19	0.21	0.25	0.22	0.13–0.21	0.09–0.27	
LOI	4.27	3.68	3.78	4.18	1.72	2.76	4.10	1.90	2.06–2.75	1.36–3.50	
TOTAL	99.81	99.53	99.44	100.01	99.90	100.05	100.33	100.11	99.65–100.18	99.65–100.60	
Trace elements(ppm)											
Cr	250	217	182	222	238	229	207	274	10.3–19.3		
Ni	31.0	21.9	38.1	21.7	23.9	34.1	26.1	28.3	4.69–10.5		
Rb	136.1	110.4	86.5	102.1	90.7	91.3	125.5	89.9	14.3–26.7	8.83–49.7	
Ba	1193	887	904	1654	1302	995	1943	1213	298–440	262–635	
Th	15.3	20.0	16.5	17.4	18.0	15.0	19.8	19.2	4.27–5.65	0.450–7.10	
U	2.61	3.84	3.40	2.19	1.69	1.32	2.04	2.33	1.41–2.01	0.160–3.79	
Nb	10.5	11.1	10.0	10.2	10.0	10.5	10.6	11.6	4.52–5.37	1.87–5.23	
Ta	0.734	0.837	0.733	0.801	0.767	0.713	0.803	0.875	0.29–0.31	0.110–0.320	
Pb	16.2	34.1	9.9	8.6	11.4	11.7	11.0	10.2	4.65–7.30		
La	49.9	44.6	33.3	28.2	16.3	21.9	32.2	25.2	17.1–30.6	9.84–33.9	
Ce	85.4	72.1	61.6	50.3	27.9	38.0	56.4	43.4	38.3–75.2	20.6–69.8	

Pr	9.40	7.84	7.26	5.92	3.23	4.46	6.62	4.96	5.19–9.64	2.58–8.80	
Sr	172	304	1145	509	696	530	788	851	122–403	145–541	
Nd	32.5	26.3	25.6	21.0	11.2	15.7	23.2	17.0	22.6–39.9	11.2–36.2	
Zr	124	126	107	140	128	98	143	150	140–208	28.0–175	
Hf	3.28	3.60	3.07	3.82	3.47	2.78	3.93	4.06	4.19–5.66	0.630–4.29	
Sm	5.68	4.18	4.63	3.83	2.02	2.87	4.27	2.98	4.44–7.25	2.06–6.51	
Eu	1.43	1.10	1.22	0.97	0.71	0.74	1.10	0.87	0.99–1.58	0.620–1.49	
Ti	2880	2520	3420	2760	2520	2760	2820	2820	2400–5040	1920–4080	
Gd	4.79	3.29	3.62	2.98	1.74	2.46	3.56	2.51	3.26–5.59	1.73–4.77	
Tb	0.64	0.45	0.53	0.44	0.24	0.34	0.49	0.34	0.57–0.73	0.250–0.680	
Dy	3.36	2.36	2.89	2.36	1.22	1.76	2.53	1.71	2.94–4.06	1.45–3.91	
Y	17.5	12.1	14.5	12.6	7.55	10.3	14.0	9.85	15.1–20.7	7.98–20.8	
Ho	0.65	0.44	0.56	0.45	0.24	0.34	0.49	0.33	0.55–0.77	0.310–0.820	
Er	1.69	1.16	1.48	1.19	0.64	0.95	1.34	0.91	1.65–2.19	0.880–2.30	
Tm	0.25	0.18	0.23	0.18	0.09	0.15	0.20	0.15	0.26–0.32	0.120–0.350	
Yb	1.57	1.13	1.48	1.19	0.62	0.99	1.36	0.97	1.71–2.19	0.880–2.31	
Lu	0.23	0.17	0.23	0.18	0.10	0.15	0.21	0.15	0.28–0.35	0.150–0.350	
δEu	0.84	0.91	0.91	0.88	1.15	0.85	0.86	0.98	0.24–0.26	0.210–0.380	
$(La/Lu)_N$	23.3	28.1	15.7	16.5	16.7	15.7	16.8	17.5	6.55–10.6	4.77–13.18	
Nb/U	4.04	2.90	2.95	4.64	5.95	7.95	5.17	4.98	2.60–3.24	0.510–14.7	
Nb/Ta	14.4	13.3	13.7	12.7	13.1	14.7	13.1	13.3	16.8–18.8	11.6–19.4	
Zr/Hf	37.7	35.1	34.7	36.5	37.0	35.1	36.4	37.0	33.4–41.0	34.1–44.4	
Sr–Nd isotope ratios											
$^{87}Rb/^{86}Sr$	2.4508		0.2128	0.5820		0.4884	0.4620				
$^{87}Sr/^{86}Sr$	0.711812		0.707110	0.708384		0.706178	0.707419				
2σ ($^{87}Sr/^{86}Sr$)	0.000015		0.000014	0.000014		0.000014	0.000014				
$^{147}Sm/^{144}Nd$	0.1029		0.1030	0.1078		0.1048	0.1057				0.121–0.168
$^{143}Nd/^{144}Nd$	0.512519		0.512518	0.512527		0.512536	0.512548				0.512488–0.512785
$2\sigma(^{143}Nd/^{144}Nd)$	0.000012		0.000011	0.000013		0.000013	0.000014				0.000008–0.000013
$I_{Sr}(t)$	0.7058		0.7066	0.7070		0.7050	0.7063				
$I_{Nd}(t)$	0.51		0.51	0.51		0.51	0.51				
$\varepsilon_{Nd}(t)$	−0.26		−0.28	−0.20		0.03	0.25				5.2–8.7
T_{DM2}(Ma)	981		983	976		957	939				840–1100(T_{DM1})

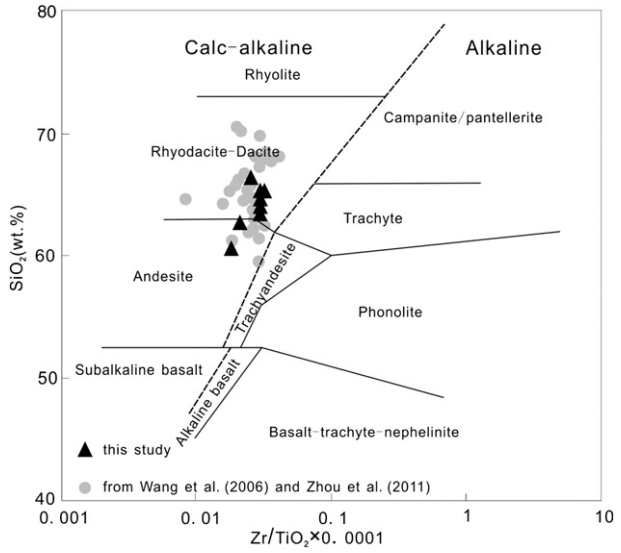

Fig. 4. Zr/TiO_2 vs. SiO_2 diagram for granodioritic porphyry at the Dexing porphyry copper deposit.
Adapted from Wang et al. (2006).

studies (Wang et al., 2006; Zhou et al., 2011). Chen and Jahn (1998) reviewed the Sr and Nd isotope characteristics of rocks from South China and constructed a Nd isotopic evolution diagram for the metamorphic basement rocks of Jiangnan Orogen. On their original diagram, the Dexing granodioritic porphyry plots in the region above that for the Shuangxiwu Group. However, the formation age used by Chen and Jahn (1998) was ~140 Ma rather than the more reliable age of ~170 Ma (Wang et al., 2006; Zhou et al., 2011; this study). Moreover, the T_{DM} of 1100–1300 Ma used by Chen and Jahn (1998) is much older than the newly obtained and more precise values of 840–1200 Ma by Li et al. (2009). In Fig. 6 we show a revised diagram incorporating the new data and on this revised Nd isotopic evolution diagram, the Dexing granodioritic porphyry plots within the same region as that of the Shuangxiwu Group, although above the region for their Shuangqiaoshan Group host rocks.

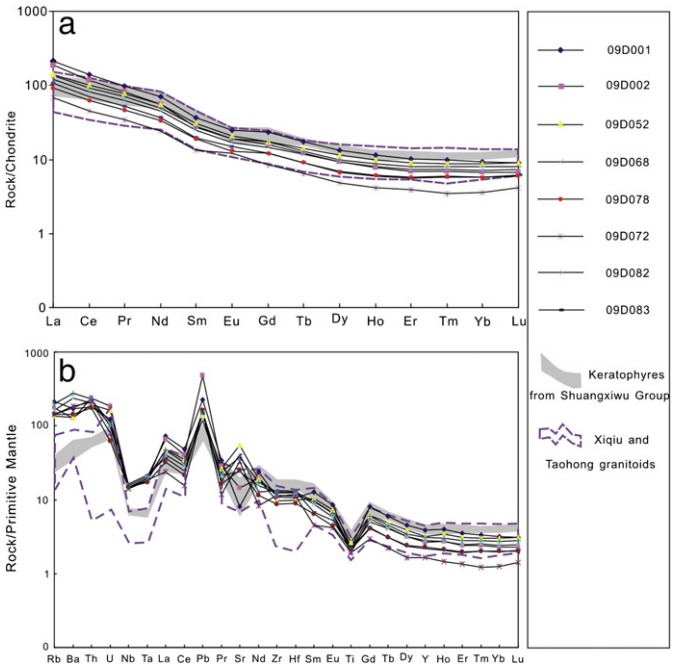

Fig. 5. a) Chondrite normalized REE distribution patterns for the granodioritic porphyry. b) Primitive mantle normalized multi-elements patterns. Both of the normalizing values are from Sun and McDonough (1989), reference data of the keratophyre are from Chen et al. (2009) and reference data of the Xiqiu–Taohong granitoids are from Ye et al. (2007).

5.4. Zircon Hf isotope

The results are listed in Supplemental Electronic Data Table 2, and the zircon CL images are shown in Fig. 2. $^{176}Lu/^{177}Hf$ ratios of all zircons from the five samples are less than 0.002 (ranging from 0.000527 to 0.001334), indicating that negligible amount of radiogenic ^{177}Hf was produced by β decay of ^{176}Lu. All the zircons except for 09D107-07 (the inherited core) show similar initial $^{176}Hf/^{177}Hf$ values ranging from 0.282722 to 0.282862, with a mean at 0.282793. Correspondingly, the calculated $\varepsilon_{Hf}(t)$ values are all positive, varying from 2.0 to 7.0, averaging at 4.6 (Fig. 7), and the two-stage depleted mantle model ages (T_{DM2}) show a range of 800–1000 Ma, clustering at ~920 Ma (Fig. 8). An exception is zircon 09D107-7 with a $^{176}Lu/^{177}Hf$ ratio of 0.000991, initial $^{176}Hf/^{177}Hf$ of 0.282740, ε_{Hf}(946 Ma) of 19.8 and single-stage depleted mantle model age of 701 Ma. On the T–$\varepsilon_{Hf}(t)$ diagram (Fig. 9), analyses of all the zircons except 09D107-7 plot in the field of evolution of the keratophyre from the Shuangxiwu Group and volcanic rocks from Pingshui Formation, Shuangxiwu Group.

5.5. Zircon oxygen isotopes

Oxygen isotopic analysis of magmatic rocks has been employed to derive information about source rocks, and this technique has a greater potential when performed on zircons since the mineral is resistant to high temperature alteration and dry granulite-facies metamorphism, and is thus capable of preserving the magmatic oxygen compositions (Zheng et al., 2004, 2008). The normal $\delta^{18}O$ value of mantle zircons is $5.3 \pm 0.3‰$ (Valley, 2003; Valley et al., 1998). Melts derived from sedimentary protoliths will have elevated $\delta^{18}O$ values, and thus zircons crystallized from such melts have $\delta^{18}O$ values higher than the mantle value. In contrast, melts originated from rocks which suffered high temperature hydrothermal alteration will be depleted in ^{18}O, and the resultant zircons will have $\delta^{18}O$ values lower than the mantle value.

In situ zircon oxygen isotope analyses by SIMS indicate that the Dexing granodioritic porphyry has uniform $\delta^{18}O$ values, ranging from 4.7 to 5.9‰ (mean at $5.4 \pm 0.1‰$, $n = 74$) (Fig. 10 and Table 3), similar to those of zircons crystallized from mantle magmas. Moreover, volcanic rocks from Shuangxiwu Group (~5.7‰, Qi et al., 1986) and the Taohong granitoids (5.7–6.1‰, Ye, 2006) also show $\delta^{18}O$ values similar to those of the zircons in the Dexing granodioritic porphyry.

6. Discussion

6.1. Magma formation age and tectonic setting

The zircons from five representative rock samples analyzed by LA-ICPMS in this study yielded weighted mean $^{206}Pb/^{238}U$ ages of 172.5 ± 0.5 Ma, which are broadly similar to the ages obtained by Wang et al. (2006) and Zhou et al. (2011) in previous studies from this region. Therefore, the Dexing granodioritic porphyry is interpreted to be formed at ca. 172.5 Ma. Although no inherited zircons were reported in previous investigations (Wang et al., 2004, 2006; Zhou et al., 2011), our present study recorded a rare inherited core dated at ~946 Ma, suggesting that the source rocks of the Dexing granodioritic porphyry were formed in the early Neoproterozoic.

The tectonic setting of the Dexing porphyry Cu deposit has been discussed by several authors. Wang et al. (2006) suggested that the Dexing porphyry Cu deposit formed in an extensional environment, as evidenced by the presence of Middle Jurassic (160–180 Ma) intra-plate alkaline basalts, gabbros, bimodal volcanic-intrusive complex and Jurassic extensional sedimentary basins in South China.

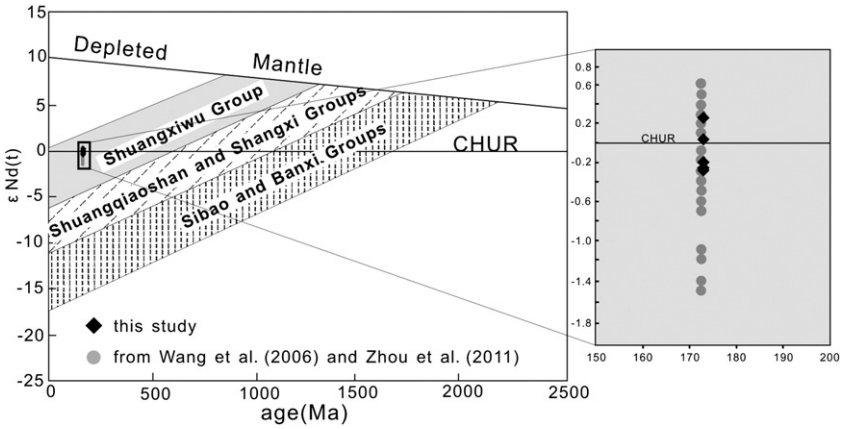

Fig. 6. Nd isotopic evolution diagram for metamorphic basement rocks in the Jiangnan Orogen (adapted from Chen and Jahn, 1998). Plots of the Dexing granodioritic porphyry are shown by the black diamonds. The inset is an enlargement of the area with 100–150 Ma for the "age" axis and −1.0–1.0 for the "εNd(t)" axis. The T_{DM} upper limit of the Shuangxiwu Group was lowered to 840 Ma according to the data from Li et al. (2009).

Furthermore, they concluded that the extension resulted from the activity of Shi-Hang rift zone. Deng et al. (2004) and Griffin et al. (1998) proposed out that the lithosphere and crust of eastern China have average thickness of 200 km and 40 km, respectively, prior to the Jurassic. However, during the time from Mid-Jurassic to Early Cretaceous (150–130 Ma), the lithosphere was thinned to 60–80 km whereas the crust was thickened to 50–60 km. Hou et al. (2011) synthesized the various observations which lead to a consensus on

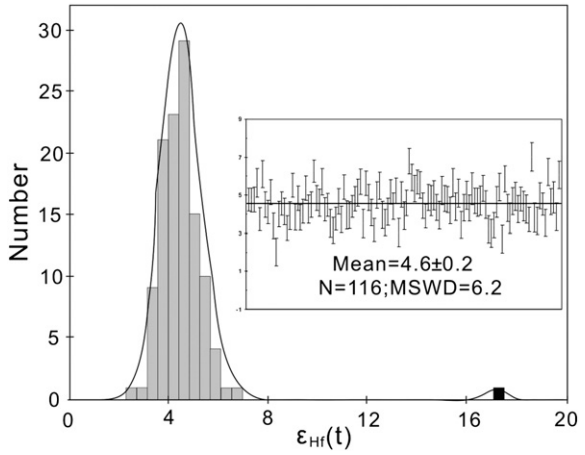

Fig. 7. Histogram showing $\varepsilon_{Hf}(t)$ values of zircons from the Dexing granodioritic porphyry. The inset shows weighted average calculation of the $\varepsilon_{Hf}(t)$. The black column was not included in calculation of mean value.

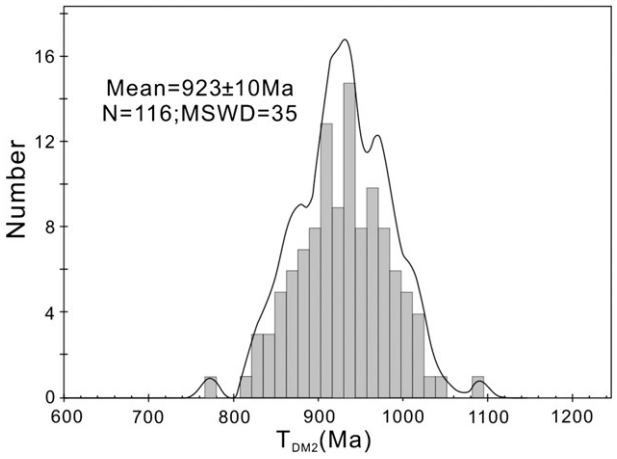

Fig. 8. Histogram showing two-stage depleted mantle model ages of zircons from the Dexing granodioritic porphyry.

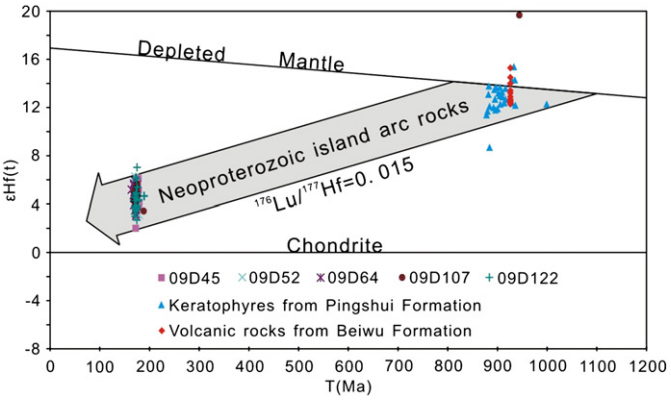

Fig. 9. T–$\varepsilon_{Hf}(t)$ diagram of zircons from the Dexing granodioritic porphyry. Reference data of the keratophyre of Pingshui Formation, Shuangxiwu Group and volcanic rocks of Beiwu Formation, Shuangxiwu Group are from Chen et al. (2009) and Li et al. (2009), respectively.

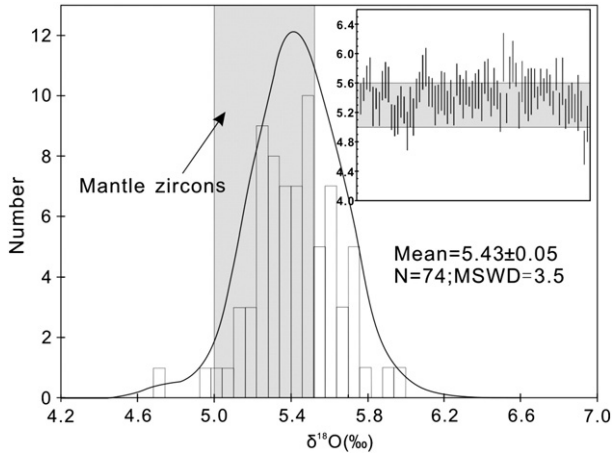

Fig. 10. Histogram showing zircon $\delta^{18}O$ values from the Dexing granodioritic porphyry. Reference $\delta^{18}O$ values of mantle zircons and volcanic rocks from the Shuangxiwu Group are from Valley et al. (1998, 2003) and Qi et al. (1986), respectively. The inset shows weighted average calculation of the $\delta^{18}O$ values.

Table 3
Results of SIMS zircon oxygen isotopic analyses of the Dexing granodioritic porphyry.

Sample	$\delta^{18}O$	2σ	Sample	$\delta^{18}O$	2σ	Sample	$\delta^{18}O$	2σ
09D45			09D52			09D64		
1	5.74	0.24	1	5.38	0.21	1	5.95	0.33
2	5.82	0.26	2	5.51	0.16	2	5.25	0.20
3	5.48	0.21	3	5.67	0.16	3	5.74	0.22
4	5.47	0.20	4	5.71	0.23	4	5.89	0.28
5	5.29	0.27	5	5.28	0.27	5	5.71	0.16
6	5.37	0.20	6	5.38	0.14	6	5.23	0.25
7	5.49	0.27	7	5.24	0.23	7	5.62	0.28
8	5.45	0.29	8	5.56	0.20	8	5.43	0.26
9	5.26	0.23	9	5.64	0.25	9	5.44	0.36
10	5.41	0.23	10	5.58	0.24	10	5.48	0.32
11	5.21	0.20	11	5.13	0.17	11	5.60	0.20
12	5.64	0.22	12	5.08	0.21	12	5.39	0.15
13	5.50	0.20	13	5.16	0.26	13	5.61	0.19
14	5.38	0.27	14	5.34	0.22	14	5.51	0.16
15	5.53	0.23	15	5.23	0.18	15	5.62	0.17
16	5.41	0.13	16	4.94	0.26	16	5.50	0.21
17	5.37	0.26	17	5.27	0.28	17	5.33	0.16
18	5.49	0.24	18	5.13	0.26	18	5.72	0.22
19	5.51	0.27	19	5.45	0.20	19	5.24	0.22
20	5.34	0.26	20	5.54	0.21	20	5.62	0.32
21	5.67	0.22				21	5.18	0.20
22	5.64	0.29				22	5.30	0.26
23	5.34	0.20				23	5.36	0.24
24	5.55	0.26				24	5.25	0.19
25	5.44	0.20				25	5.33	0.38
26	5.20	0.27				26	5.28	0.21
						27	4.71	0.23
						28	5.04	0.25

intense crustal thickening that probably started in the Mid-Triassic and continued until the Early–Middle Jurassic, followed by large-scale thinning of the sub-continental lithospheric mantle (SCLM) in eastern China, and leading to either SCLM delamination or asthenospheric upwelling.

From the age data presented in this study and in other recent studies, it is evident that the Dexing granodioritic porphyry was formed during the Middle Jurassic when lithospheric thinning triggered by either asthenospheric upwelling or sub-continental lithospheric mantle delamination had occurred.

6.2. Assessment of the existing models of magma genesis

The petrogenesis of Dexing granodioritic porphyry has been attempted in various studies during the last three decades, and many models have been proposed. The early research primarily focused on geochemical and Sr–Nd isotopic features and the conclusions reached include, 1) depleted mantle derived magmas (Qian and Lu, 2005; Rui et al., 1984; Zhu et al., 1983) and 2) magma derived by the mixing of mantle and crustal materials (Chen and Jahn, 1998; Zhu et al., 1990, 2002). Although several models have been proposed for the magma tectonics, here we focus mainly on the models presented in Hou et al. (2011), Sun et al. (2010) and Wang et al. (2006).

On the basis of geochemical and Sr–Nd isotopic investigation, Wang et al. (2006) proposed that the Dexing granodioritic porphyry possesses adakitic signatures, with elevated Cr, Ni contents and high $Mg^{\#}$. They suggested that these signatures were produced by melting of a delaminated lower crust and equilibration of the melts within the lithospheric mantle. Furthermore, Wang et al. (2006) believed that the resulted melts led to an elevation of oxidation state of the mantle and thus mobilized Cu from the mantle. Their model seems to provide a good explanation on the geochemical and isotopic characters observed, but could be debated because of two major reasons. Firstly, it is difficult for partial melting to occur in a delaminated lower crust when pressure is significantly increased (Zhang et al., 2006, 2008); also there is no geological evidence to support the lower crustal delamination model (Hou et al., 2011; Zhang et al., 2008). Secondly, melting of the delaminated lower crust should have triggered a large scale of contemporaneous magmatism, but magmatic rocks of ~170 Ma are not common in the Dexing area.

Recent models have proposed that adakites formed by partial melting of subducted oceanic crust are responsible for the formation of many of the porphyry ore deposits (Oyarzun et al., 2001; Sajona and Maury, 1998; Thiéblemont et al., 1997). There are ongoing debates about this topic (Castillo, 2006; Richards and Kerrich, 2007; and reference therein). A similar model is also being widely adopted for related ore deposits in China (Hou and Yang, 2009; Hou et al., 2001, 2003, 2004, 2005; Leng et al., 2007; Sun et al., 2010; Wang et al., 2004, 2006; Xu et al., 2002; Zhang et al., 2001, 2004). Sun et al. (2010) proposed that the Lower Yangtze metallogenic belt and the Dexing porphyry Cu deposit were associated with slab melts generated during ridge subduction of the paleo-Pacific ocean at ~140 Ma. However, precise geochronological data show that the Dexing granodioritic porphyry was formed at ~170 Ma, significantly earlier than the proposed timing of subduction. Rosenbaum et al. (2005) investigated the influence of subduction of the Nazca ridge and Inca Plateau beneath the South American plate on the spatial and temporal distribution of ore deposits in that region. Their results show a rapid metallogenic response to the arrival of the topographic anomalies at the subduction trench. They suggested that flattening of the subducting oceanic slab which is capable of leading to generation of adakites can be one explanation for the relationship between ridge subduction and porphyry copper deposit formation. But they concluded that an important factor for ore formation was the change of the state of stress in the crust (enhanced seismicity and crustal deformation), and flat subduction was not the primary mechanism controlling ore formation. Rosenbaum and Mo (2011) further suggested that flattening of slab is only significant in the eastern Pacific where the average slab dip angle is shallow. In contrast, in the western Pacific the average subduction angle is steeper and there is no significant flatting of the dip angle. In this respect, ridge subduction cannot adequately explain the formation of the Dexing porphyry Cu deposit.

Hou et al. (2011), in their recent synthesis, suggested that the Dexing granodioritic porphyry shows adakitic affinity, and was generated by partial melting of a thickened mafic lower crust (50–60 km) infiltrated by small batches of juvenile mantle magmas. Several lines of evidence have been incorporated into their model, but the authors did not address the arc-like magmatic signatures of the Dexing porphyry, and in particular the enrichment in fluid mobile elements, and the depletion in fluid immobile elements (e.g. Nb, Ta, and Ti). In addition, they suggested that Cu was brought in by mantle "patches" infiltrated into the mafic crust, but this idea is not supported by any geochemical or geological evidence. In comparison, Richards (2009, 2011) proposed genetic models for "post-subduction porphyry copper deposits". In his models, the fertile magmas are considered to have been generated by the melting of subduction-modified upper plate lithosphere, which may remobilize metals and other elements introduced during the first-stage arc magmatism. In the case of melting lower crustal rocks, the resulting magmas are commonly calc-alkaline and may have crustal radiogenic isotopic signatures. If amphibole and/or garnet were present in the lower crustal, the former arc source rocks may produce high Sr/Y and La/Yb characters for the magmas. This model is therefore closer to the geological, geochemical and isotopic data from the Dexing porphyry copper deposit.

6.3. Source of magmas

The major and trace element data from the Dexing granodioritic porphyry presented in this study show that the rock is rich in fluid mobile elements but depleted in fluid immobile elements. Commonly, these signatures are diagnostic of volcanic arc magmas. However, it has been demonstrated that the Dexing porphyry copper deposit

was formed in a non-arc setting. In this case, it is important to address how the Dexing porphyry acquired the arc-like trace element features. The Xucun, Xiuning and Shexian granitoids which formed at ~820 Ma in the eastern part of the Jiangnan Orogen in south Anhui, are typical S-type granites, although they exhibit arc-like trace element characteristics. Wu et al. (2006) suggested that they were generated by remelting of a juvenile arc lower crust in a tectonic setting of arc–continent collision, and this means that the arc-like signatures were inherited from their source rocks. The volcanic rocks of the Shuangxiwu Group (Chen et al., 2009; Cheng, 1993; Li et al., 2009; Qi et al., 1986; Zhou, 1992) and associated intrusive rocks (Li et al., 2009; Qi et al., 1986; Ye et al., 2007) are considered to represent a suite of arc magmatic rocks generated during oceanic subduction in the early Neoproterozoic. The Dexing granodioritic porphyry exhibits trace element signatures which are remarkably similar to those of the volcanic rocks from the Shuangxiwu Group and its associated intrusive rocks. This suggests that the Dexing granodioritic porphyry might have been sourced from the Neoproterozoic arc lower crustal rocks. This inference is further supported by Nd, Hf, and O isotopic data.

As mentioned previously, the adakitic nature of the Dexing granodiorite has been observed by several authors (Hou et al., 2011; Wang et al., 2004, 2006). Wang et al. (2006) suggested that the rock was generated by melting of a delaminated lower crust in lithospheric mantle where garnet was stable. In contrast, Hou et al. (2011) summarized that the lower crust in eastern China is mafic and was thickened to 50–60 km (garnet amphibolite facies) during late Triassic and Mid-Jurassic. Melting of this hydrous and thickened crust could account for the origin of Dexing granodioritic porphyry. As a matter of fact, there exist other explanations for adakitic signatures. Gao et al. (2009) discovered an adakitic signature from the mafic enclave-bearing plagiogranites from this region and considered that these rocks formed by the fractional crystallization of hornblende and accessory minerals such as apatite and ilmenite from the parental magmas. Recently, we have found a small number of mafic enclaves in the Dexing granodioritic porphyry, but further geochemical analyses have not been conducted yet. It is likely that the adakitic signatures were generated by those mafic enclaves. Before verification of the above assumption, we adopt explanation of partial melting of thicken source rocks for the adakitic signatures.

More convincingly, the bulk-rock Nd and zircon Hf analyses presented in our study further suggest that the Dexing granodioritic porphyry was derived from the partial melting of lower crustal rocks of a relict Neoproterozoic island arc represented by the Shuangxiwu Group and its associated intrusive rocks. The Dexing granodioritic porphyry has positive $\varepsilon_{Hf}(t)$ values (2–7, average = 4.6), suggesting mantle-derived components in its source region. The relevant $T_{DM,2}$ values of ~900 Ma reflect that the source rocks were extracted from the depleted mantle in the early Neoproterozoic. Furthermore, comparability of Nd, Hf isotopic compositions between the Dexing granodiorite and Shuangxiwu rocks suggests that the lower crustal rocks of the Neoproterozoic island arc could be a potential source.

In accordance with the Nd and Hf isotopes, the mantle-like zircon $\delta^{18}O$ values (4.7–5.9‰) of the Dexing granodioritic porphyry suggest that their source region consisted of depleted mantle-derived magmatic rocks, and that no major sedimentary protoliths were involved in the magma genesis, nor did the magmas witness high temperature hydrothermal fluids. Our inferences contradict the model proposed by Zhou et al. (2011), who suggested that the Dexing granodioritic porphyry mainly originated from partial melting of sedimentary rocks on the subducted ocean floor. Qi et al. (1986) reported a $\delta^{18}O$ value of 5.7‰ for volcanic rocks from the Shuangxiwu Group, and Ye (2006) reported $\delta^{18}O$ values of 5.7–6.1‰ and 5.9–7.6‰ for the Xiqiu and Taohong granitoids. The oxygen isotopes of the Dexing granodioritic porphyry are broadly similar to the values of those Neoproterozoic arc-derived rocks.

Spatially, the Qigong Group, commonly regarded as counterpart rocks of the Shuangxiwu Group in Jiangxi, is distributed near the Dexing deposit, and this indicates that the underlying relict arc rocks spatially have the potential to be the source rocks of the Dexing granodioritic porphyry. In addition, the NEJF is a deep fault transecting into the mantle/crust boundary. It is believed to have been controlling regional magma transportation since its formation (Zhu et al., 1983). Therefore, NEJF was likely to serve as a passage for magmas that were generated by partial melting of the relict arc rocks.

In conclusion, the geochemical and isotopic similarities as well as close spatial relationship between the Dexing granodioritic porphyry and the Neoproterozoic arc rocks suggest that the ore-forming magmas of the Dexing porphyry copper deposit were generated by partial melting of the lower crustal rocks comprising the remnants of a Neoproterozoic island arc.

6.4. Source of Cu

In convergent margins, Cu is predominantly derived from partial melting of the mantle wedge metasomatized by slab fluids (Richards, 2003, references therein). Although several researchers suggested a direct relationship of porphyry copper deposits with slab derived melts, this interpretation has been challenged (Richards, 2003, 2009, 2011). In non-arc settings, the source of Cu has been a subject of debate. Hou et al. (2011) suggested that key factors that generate fertile magmas in non-arc settings are most likely crust–mantle interaction processes, and that metals like Cu and Au in the magmas are likely sourced from mantle-derived components and/or melts, which either previously underplated and infiltrated at the base of the thickened crust, or were introduced into the primitive magmas by melt/mantle interaction. In contrast, Richards (2009, 2011) suggested that metals such as copper in post-subduction porphyry Cu deposits might have been sourced from residual sulfides left at the base of the crust by arc magmas. Both the above two hypotheses are possible explanations for the origin of Cu in non-arc porphyry copper deposit. However, we prefer the latter one because our data suggest that the Dexing ore-forming magmas were generated by melting of lower crustal rocks comprising the remnants of a Neoproterozoic arc, which is similar to the model described by Richards (2009). Furthermore, our results suggest that such melting adequately explains the observed features without the requirement of any major input from the mantle. Finally, a VMS-type Cu deposit (dated at ~900 Ma on hydrothermal zircons by LA-ICPMS, Li et al., 2010a) termed the "Pingshui Cu deposit" occurs within the Pingshui Formation of Shuangxiwu Group, which has been shown to be a product of the Neoproterozoic arc magmatism (Huang, 1992; Wang and Zhao, 1980; Xu et al., 2000). This suggests that the lower crustal rocks with relicts of a Neoproterozoic island arc have the potential to generate the copper sources of the Dexing porphyry Cu deposit.

6.5. Melting of Neoproterozoic relict island arcs

Element chemistry and isotopic investigations of the Dexing granodioritic porphyry suggest that it formed through partial melting of arc roots of probably basaltic composition generated by Neoproterozoic oceanic subduction (prior to 900 Ma) leading to the generation of the Shuangxiwu and Qigong volcanic rocks and the associated intrusives, and also the Pingshui Cu deposit. The crustal rocks might represent the hydrous residues left by previous arc magmas at the base of the crust, enriched in sulfide phases. Subsequent continent–arc–continent (Charvet et al., 1998) or continent–arc–arc (Guo et al., 1996) collision led to the formation of JSF and NEJF, and preservation of the arc-related lower crustal rocks at the crust/mantle boundary. During the time between Mid-Triassic and Mid-Jurassic, these rocks were thickened and metamorphosed probably to garnet amphibolite facies, followed by large scale lithospheric thinning through the delamination of the sub-continental lithospheric mantle or through asthenospheric upwelling. The lower crustal rocks were partially melted (probably

because of their hydrous nature) with garnet and amphibole in the source, through heat input from the upwelling asthenosphere. The resulting magmas ascended along the NEJF and intruded into the Shuangqiaoshan Group in the Jiuling terrane. Cu precipitation was aided by the subsequent magma cooling and fluid exsolution. We show in Fig. 11 the schematic model to explain the various stages.

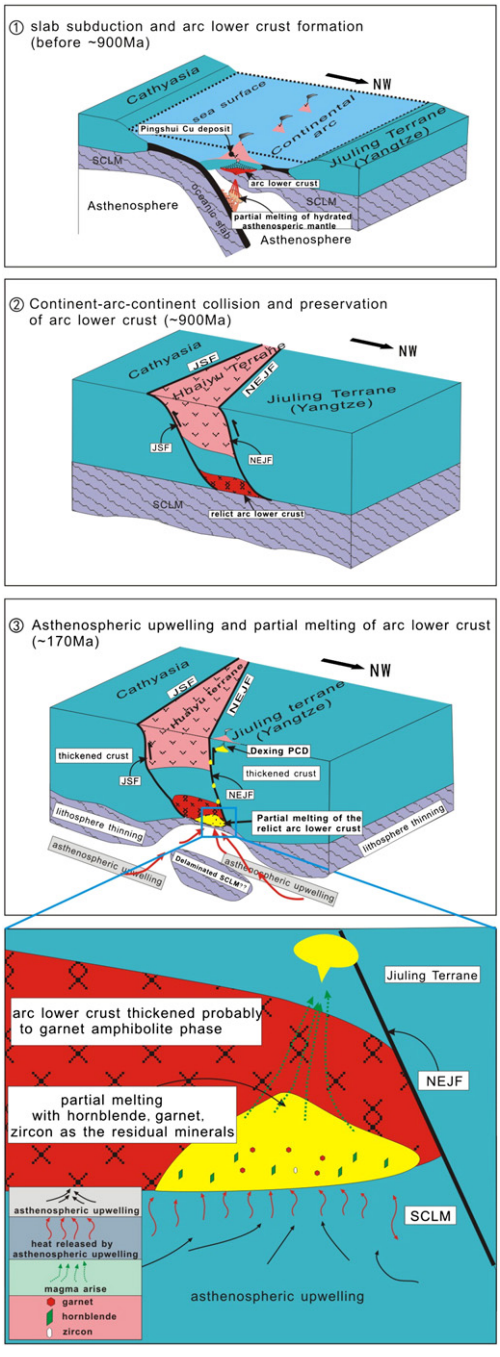

Fig. 11. Schematic model illustrating the various stages to explain the genesis of the Dexing porphyry copper deposit through the melting of the roots of a remnant Neoproterozoic island arc. (1) Oceanic slab subduction between Yangtze and Cathaysia, and formation of island arcs along the margin of Yangtze at the time before 900 Ma (adapted from Charvet et al., 1996; Richards, 2011). (2) Continent–arc–continent collision at ~900 Ma, which led to the formation of JSF and NEJF, and the preservation of the previous arc lower crustal rocks. (3) The thickened arc lower crustal rocks were partially melted by heat input from the upwelling asthenosphere, leaving hornblende, garnet and zircon in the residue. The Dexing porphyry copper deposit finally formed at ~170 Ma. SCLM: sub-continental lithospheric mantle; JSF: Jiangshan-Shaoxing fault; NEJF: northeast Jiangxi fault; PCD: porphyry copper deposit.

7. Conclusions

The Dexing Cu deposit is a typical non-arc porphyry ore deposit. LA-ICPMS U–Pb dating of zircons from the granodioritic porphyry together with the data presented in previous studies suggests that the porphyry formed in the mid-Jurassic, probably associated with lithospheric thinning triggered by sub-continental lithospheric mantle delamination or asthenospheric upwelling. The ore-forming porphyry shows both arc-like and adakitic trace element signatures, and has characteristics that are broadly similar to those of the Neoproterozoic arc rocks in the vicinity. Furthermore, the whole rock Nd, zircon Hf and O isotopes of the Dexing granodioritic porphyry are comparable to those of the proximal Neoproterozoic arc rocks. In addition, the occurrence of the Pingshui VMS-type deposit lends further support for the potential of Cu in the roots of the arc. All these features lead us to conclude that the Dexing porphyry copper deposit is a product of partial melting of the relict Neoproterozoic island arcs.

Supplementary data to this article can be found online at http://dx.doi.org/10.1016/j.lithos.2012.05.018.

Acknowledgments

We are grateful to Chao-Feng Li and Xiang-Hui Li for help during Sr and Nd isotope analyses, Zhao-Chu Hu for help during zircon LA-ICPMS U–Pb dating, and Xian-Hua Li for help during zircon oxygen analysis. Dr. Hong Zhang, three anonymous reviewers and the guest Editor Dr. Weidong Sun are thanked for their constructive and valuable comments which greatly contributed to the improvement of the manuscript. This study was financially supported by the Intellectual Innovation Project, Chinese Academy of Sciences (KZCX1-YW-15-3).

References

Blichert-Toft, J., Albarède, F., 1997. The Lu–Hf isotope geochemistry of chondrites and the evolution of the mantle–crust system. Earth and Planetary Science Letters 148, 243–258.
Castillo, P.R., 2006. An overview of adakite petrogenesis. Chinese Science Bulletin 51, 258–268.
Charvet, J., Shu, L.S., Shi, Y.S., Guo, L.Z., Faure, M., 1996. The building of south China: collision of Yangzi and Cathaysia blocks, problems and tentative answers. Journal of Southeast Asian Earth Sciences 13, 223–235.
Chen, J.F., Jahn, B.M., 1998. Crustal evolution of southeastern China: Nd and Sr isotopic evidence. Tectonophysics 284, 101–133.
Chen, J.F., Foland, K.A., Xu, X., Zhou, T.X., 1991. Magmatism along the southeast margin of the Yangtze block: Precambrian collision of the Yangtze and Cathaysia blocks of China. Geology 19, 815–818.
Chen, Z.H., Xing, G.F., Guo, K.Y., Dong, Y.G., Chen, R., Zeng, Y., Li, L.M., He, Z.Y., Zhao, L., 2009. Petrogenesis of keratophyres in the Pingshui Group, Zhejiang: constraints from zircon U–Pb ages and Hf isotopes. Chinese Science Bulletin 54, 1570–1578.
Cheng, H., 1993. Geochemistry of Proterozoic island-arc volcanic rocks in northwest Zhejiang. Geochimica 22, 18–27 (in Chinese with English abstract).
Defant, M.J., Drummond, M.S., 1990. Derivation of some modern arc magmas by melting of young subducted lithosphere. Nature 347, 662–665.
Deng, J.F., Luo, Z.H., Su, S.H., Mo, X.X., Yu, B.S., Lai, X.Y., Kan, H.W., 2004. Rock Genesis, Tectonic Settings and Metallogeny. Geological Publishing House, Beijing. 380 pp. (in Chinese with English abstract).
Faure, G., 1977. Principles of Isotope Geology. John Wiley and Sons, New York, pp. 156–180.
Gao, J., Klemd, R., Long, L.L., Xiong, X.M., Qian, Q., 2009. Adakitic signature formed by fractional crystallization: an interpretation for the Neo-Proterozoic meta-plagiogranites of the NE Jiangxi ophiolitic mélange belt, South China. Lithos 110, 277–293.
Griffin, W.L., Zhang, A.D., O'Reilly, S.Y., Ryan, G., 1998. Phanerozoic evolution of the lithosphere beneath the Sino-Korean Craton. In: Flower, M., Chung, S.L., Lo, C.H., Lee, T.Y. (Eds.), Mantle Dynamics and Plate Interaction in East Asia: American Geophysical Union Geodynamic Series, 27, pp. 107–126.
Griffin, W.L., Pearson, N.J., Belousova, E., Jackson, S.E., van Achterbergh, E., O'Reilly, S.Y., Shee, S.R., 2000. The Hf isotope composition of cratonic mantle: LAM-MC-ICPMS analysis of zircon megacrysts in kimberlites. Geochimica et Cosmochimica Acta 64, 133–147.
Guo, L.Z., Shi, Y.S., Lu, H.F., Ma, R.S., Sun, Y., Shu, L.S., Jia, D., Zhang, Q.L., 1996. On the Meso-Neoproterozoic Jiangnan island arc: its kinematics and dynamics. Geological Journal of University 2, 1–13 (in Chinese with English abstract).
Hou, Z.Q., Yang, Z.M., 2009. Porphyry deposits in continental settings of China: geological characteristics magmatic–hydrothermal system, and metallogenic model. Acta Geologica Sinica 83, 1779–1817 (in Chinese with English abstract).
Hou, Z.Q., Qu, X.M., Huang, W., Gao, Y.F., 2001. Modes of occurrence of gold in supergene medium in arid areas of northern China. Chinese Geology 28, 27–30 (in Chinese with English abstract).

Hou, Z.Q., Qu, X.M., Wang, S.X., Gao, Y.F., Du, A.D., Huang, W., 2003. Science in China (Series D) 33, 609–619 (in Chinese with English abstract).
Hou, Z.Q., Gao, Y.F., Meng, X.J., Qu, X.M., Huang, W., 2004. Genesis of Adakitic porphyry and tectonic controls on the Gangdese Miocene porphyry copper belt in the Tibetan Orogen. Acta Petrologica Sinica 20, 239–248 (in Chinese with English abstract).
Hou, Z.Q., Meng, X.J., Qu, X.M., Gao, Y.F., 2005. Copper ore potential of adakitic intrusives in Gangdese porphyry copper belt: constrains from rock phase and deep melting process. Mineral Deposits 24, 108–121 (in Chinese with English abstract).
Hou, Z.Q., Mo, X.X., Yang, Z.M., Wang, A.J., Pan, G.T., Qu, X.M., Nie, F.J., 2006a. Metallogeneses in the collisional Orogen of the Qinghai–Tibet plateau: tectonic setting, tempo-spatial distribution and ore deposit types. Geology in China 33, 340–352 (in Chinese with English abstract).
Hou, Z.Q., Yang, Z.S., Xu, W.Y., Mo, X.X., Ding, L., Gao, Y.F., Dong, F.L., Li, G.M., Qu, X.M., Zhao, Z.D., Jiang, S.H., Meng, X.J., Li, Z.Q., Qin, K.Z., Yang, Z.M., 2006b. Metallogenesis in Tibetan collisional orogenic belt: I. Mineralization in main collisional orogenic setting. Mineral Deposits 25, 337–358 (in Chinese with English abstract).
Hou, Z.Q., Pan, X.F., Yang, Z.M., Qu, X.M., 2007. Porphyry Cu–(Mo–Au) deposits no related to oceanic-slab subduction: examples from Chinese porphyry deposits in continental settings. Geoscience 21, 332–351 (in Chinese with English abstract).
Hou, Z.Q., Zhang, H.R., Pan, X.F., Yang, Z.M., 2011. Porphyry Cu(–Mo–Au) deposits related to melting of thickened mafic lower crust: examples from the eastern Tethyan metallogenic domain. Ore Geology Reviews 39, 21–45.
Huang, Y.N., 1992. Characteristics of Xiqiu Cu–Massive sulfide deposit, Zhejiang and the metallogenic model. Contributions to Geology and Mineral Resources Research 7, 22–34.
Humphries, S.E., 1984. The mobility of the rare earth elements in the crust. In: Henderson, P. (Ed.), Rare Earth Element Geochemistry. Elsevier, Armsterdam, pp. 315–341.
Humphris, S.E., Thompson, G., 1978. Trace element mobility during hydrothermal alteration of oceanic basalts. Geochimica et Cosmochimica Acta 42, 127–136.
Jin, Z.D., 1999. Geochemistry and evolution of ore-forming fluids at Tongchang porphyry copper deposit, Dexing County, Jiangxi province. PhD dissertation, Nanjing University, 1-124 (in Chinese with English abstract).
Jin, Z.D., Zhu, J.C., Li, F.C., 2002. O, Sr and Nd isotopic tracing of ore-forming process in Dexing porphyry copper deposit, Jiangxi province. Mineral Deposits 21, 342–349 (in Chinese with English abstract).
Kelepertsis, A.E., Esson, J., 1987. Major-and trace-element mobility in altered volcanic rocks near Stypsi, Lesbos, Greece and genesis of a kaolin deposit. Applied Clay Science 2, 11–28.
Lan, T.G., Fan, H.R., Hu, F.F., Tomkins, A.G., Yang, K.F., Liu, Y.S., 2011. Multiple crust–mantle interactions for the destruction of the North China Craton: geochemical and Sr–Nd–Pb–Hf isotopic evidence from the Longbaoshan alkaline complex. Lithos 122, 87–106.
Leng, C.B., Zhang, C.X., Chen, Y.J., Wang, S.X., Gou, T.Z., Chen, W., 2007. Discussion on the relationship between Chinese porphyry copper deposits and adakitic rocks. Earth Science Frontiers 14, 199–210 (in Chinese with English abstract).
Li, X.F., Sasaki, M., 2007. Hydrothermal alteration and mineralization of middle Jurassic Dexing porphyry Cu–Mo deposit, southeast China. Resource Geology 57, 409–426.
Li, X.H., Zhou, G.Q., Zhao, J.X., 1994. SHRIMP ion microprobe zircon U–Pb age of the NE Jiangxi ophiolite and its tectonic implications. Geochimica 23, 125–132 (in Chinese with English abstract).
Li, X.H., Li, Z.X., Ge, W.C., Zhou, H.W., Li, W.X., Liu, Y., 2001. U–Pb zircon ages of the Neoproterozoic granitoids in South China and their tectonic implications. Bulletin of Mineralogy, Petrology and Geochemistry 20, 271–273 (in Chinese with English abstract).
Li, X.H., Li, W.X., Li, Z.X., Lo, C.H., Wang, J., Ye, M.F., Yang, Y.H., 2009. Amalgamation between the Yangtze and Cathaysia Blocks in South China: constraints from SHRIMP U–Pb zircon ages, geochemistry and Nd–Hf isotopes of the Shuangxiwu volcanic rocks. Precambrian Research 174, 117–128.
Li, C.H., Xing, G.F., Jiang, Y.H., Dong, Y.G., Yu, X.M., Chen, Z.H., Jiang, Y., Chen, R., 2010a. LA-ICPMS U–Pb dating of zircons from sulfides-bearing quartz veins in the Pingshui copper deposit, Zhejiang province, and its geological implications. Geology in China 37, 477–487 (in Chinese with English abstract).
Li, X.H., Li, W.X., Li, Q.L., Wang, X.C., Liu, Y., Yang, Y.H., 2010b. Petrogenesis and tectonic significance of the 850 Ma Gangbian alkaline complex in South China: evidence from in situ zircon U–Pb dating, Hf–O isotopes and whole-rock geochemistry. Lithos 114, 1–15.
Lin, H.F., Zhang, B.D., Shen, W.Z., Zhang, Z.H., 1993. Crustal basement evolution of the Zhejiang-Jiangxi portion of the Jiangnan Proterozoic island arc zone. Geotectonica et Metallogenia 17, 147–152 (in Chinese with English abstract).
Liu, Y.S., Hu, Z.C., Gao, S., Günther, D., Xu, J., Gao, C.G., Chen, H.H., 2008. In situ analysis of major and trace elements of anhydrous minerals by LA-ICP-MS without applying an internal standard. Chemical Geology 257, 34–43.
Liu, Y., Gao, S., Hu, Z., Gao, C., Zong, K., Wang, D., 2010a. Continental and oceanic crust recycling-induced melt–peridotite interactions in the Trans-North China Orogen: U–Pb dating, Hf isotopes and trace elements in zircons of mantle xenoliths. Journal of Petrology 51, 537–571.
Liu, Y., Hu, Z., Zong, K., Gao, C., Gao, S., Xu, J., Chen, H., 2010b. Reappraisement and refinement of zircon U–Pb isotope and trace element analyses by LA-ICP-MS. Chinese Science Bulletin 55, 1535–1546.
Liu, X., Fan, H.R., Hu, F.F., Hu, B.G., Zhu, X.Y., 2011. SEM-EDS investigation of daughter minerals of fluid inclusions at the Dexing porphyry Cu–Mo deposit, Jiangxi province, China. Acta Petrologica Sinica 27, 1397–1409 (in Chinese with English abstract).
Lowell, J.D., Guilbert, J.M., 1970. Lateral and vertical alteration-mineralization zoning in porphyry ore deposit. Economic Geology 65, 373–408.
Ludwig, K.R., 2003. User's Manual for Isoplot 3.00. : A Geochronological Toolkit for Microsoft Excel, 4. Berkeley Geochronology Center, Special Publication, pp. 25–32.
Mao, J.W., Wang, Z.L., 2000. A preliminary study on time limits and geodynamic setting of large-scale metallogeny in east China. Mineral Deposits 19, 289–296 (in Chinese with English abstract).
McHenry, L.J., 2009. Element mobility during zeolitic and argillic alteration of volcanic ash in a closed-basin lacustrine environment: case study Olduvai Gorge, Tanzania. Chemical Geology 265, 540–552.
Oyarzun, R., Márquez, A., Lillo, J., López, I., Rivera, S., 2001. Giant versus small porphyry copper deposits of Cenozoic age in northern Chile: adakitic versus normal calc-alkaline magmatism. Mineralium Deposita 36, 794–798.
Pan, X.F., Song, Y.C., Wang, S.X., Li, Z.Q., Yang, Z.M., Hou, Z.Q., 2009. Evolution of hydrothermal fluid of Dexing Tongchang copper–gold porphyry deposit. Acta Geologica Sinica 12, 1929–1950 (in Chinese with English abstract).
Pandarinath, K., Dulski, P., Torres-Alvarado, I.S., Verma, S.P., 2008. Element mobility during the hydrothermal alteration of rhyolitic rocks of the Los Azufres geothermal field, Mexico. Geothermics 37, 53–72.
Qi, Q., Zhou, X.M., Wang, D.Z., 1986. The origin of the spilite–keratophyre series and the characteristic of the related mantle-derived granitic rocks in Xiqiu Zhejiang. Acta Petrologica et Mineralogica 5, 299–308 (in Chinese with English abstract).
Qian, P., Lu, J.J., 2005. The material resources of granodioritic porphyry in the Dexing copper ore district: a case study on trace elements. Contributions to Geology and Mineral Resources Research 20, 75–80 (in Chinese with English abstract).
Qian, P., Lu, J.J., Yao, C.L., 2003. Origin and evolution of ore-forming fluids of the Dexing porphyry copper deposit, Eastern China: fluid inclusion study. Journal of Nanjing University (Natural Science) 39, 319–326 (in Chinese with English abstract).
Richards, J.P., 2003. Tectono-magmatic precursors for porphyry Cu–(Mo–Au) deposit formation. Economic Geology 98, 1515–1533.
Richards, J.P., 2009. Post-subduction porphyry Cu–Au and epithermal Au deposits: products of remelting of subduction-modified lithosphere. Geology 37, 247–250.
Richards, J.P., 2011. Magmatic to hydrothermal metal fluxes in convergent and collided margins. Ore Geology Reviews 40, 1–26.
Richards, J.P., Kerrich, R., 2007. Special paper: Adakite-like rocks: their diverse origins and questionable role in metallogenesis. Economic Geology 102, 537–576.
Rollinson, H.R., 1993. Using Geochemical Data: Evaluation, Presentation, Interpretation. Longman Science & Technical, UK, pp. 120–121.
Rosenbaum, G., Mo, W., 2011. Tectonic and magmatic responses to the subduction of high bathymetric relief. Gondwana Research 19, 571–582.
Rosenbaum, G., Giles, D., Saxon, M., Betts, P.G., Weinberg, R.F., Duboz, C., 2005. Subduction of the Nazca ridge and the Inca plateau: insights into the formation of ore deposits in Peru. Earth and Planetary Science Letters 239, 18–32.
Rui, Z.Y., Huang, C.K., Qi, G.M., Xu, Y., Zhang, H.T., 1984. Porphyry Copper (Molybdenite) Deposits of China. Geological Publishing House, Beijing, pp. 242–252 (in Chinese with English abstract).
Sajona, F.G., Maury, R.C., 1998. Association of adakites with gold and copper mineralization in the Philippines. Comptes rendus de l'Académiedes sciences. Série II, Sciences de la terre et des planètes 326, 27–34.
Scherer, E., Munker, C., Mezger, K., 2001. Calibration of the lutetium–hafnium clock. Science 293, 683–687.
Shen, W.Z., Lin, H.F., Zhang, B.D., 1993. Sm–Nd isotopic studies of metamorphic basement rocks of the Jiangnan Proterozoic paleo-island arc. Journal of Nanjing University (Natural Sciences) 29, 460–467 (in Chinese with English abstract).
Shi, Y., Shu, L., Brewer, R.C., Charvet, J., Guo, L., 1994. Late Proterozoic terrane tectonics in the central Jiangnan belt, southeast China. Journal of South American Earth Sciences 7, 367–375.
Sillitoe, R.H., 2010. Porphyry copper systems. Economic Geology 105, 3–41.
Sturchio, N.C., Muehlenbachs, K., Seitz, M.G., 1986. Element redistribution during hydrothermal alteration of rhyolite in an active geothermal system: Yellowstone drill cores Y-7 and Y-8. Geochimica et Cosmochimica Acta 50, 1619–1631.
Sun, S.S., McDonough, W.F., 1989. Chemical and isotopic systematics of oceanic basalts: implications for mantle composition and processes. In: Saunders, A.D., Norry, M.J. (Eds.), Magmatism in the Oceanic Basalts. Geological Society Special Publication, pp. 313–345.
Sun, W.D., Lin, M.X., Yang, X.Y., Fan, Y.M., Ding, X., Liang, H.Y., 2010. Ridge subduction and porphyry copper gold mineralization: an overview. Science China Earth Science 40, 127–137.
Thiéblemont, D., Stein, G., Lescuyer, J.L., 1997. Gisements épithermauxet porphyriques: la connexion adakite: C.R. Acad. Sci. Paris, Sciences de la terre et des planètes. Earth and Planetary Sciences 325, 103–109.
Valley, J.W., 2003. Oxygen isotopes in zircon. Reviews in Mineralogy and Geochemistry 53, 343–385.
Valley, J.W., Kinny, P.D., Schulze, D.J., Spicuzza, M.J., 1998. Zircon megacrysts from Kimberlite: oxygen isotope heterogeneity among mantle melts. Contributions to Mineralogy and Petrology 133, 1–11.
Wang, H.Z., 1986. Chapter 5, the Proterozoic; chapter 6, the Sinian system. In: Yang, Z.Y., Chen, Y.Q., Wang, H.Z. (Eds.), The Geology of China. Clarendon Press, Oxford, pp. 31–63.
Wang, Z.J., Zhao, X.F., 1980. Characteristics and origin of Xiqiu copper deposit. Geology and Prospecting 19–25 (in Chinese with English abstract).
Wang, Q., Zhao, Z.H., Jian, P., Xu, J.F., Bao, Z.W., Ma, J.L., 2004. SHRIMP zircon geochronology and Nd–Sr isotopic geochemistry of the Dexing granodioritic porphyries. Acta Petrologica Sinica 20, 315–324 (in Chinese with English abstract).
Wang, Q., Xu, J.F., Jian, P., Bao, Z.W., Zhao, Z.H., Li, C.F., Xiong, X.L., Ma, J.L., 2006. Petrogenesis of adakitic porphyries in an extensional tectonic setting, Dexing, South China: implications for the genesis of porphyry copper mineralization. Journal of Petrology 47, 119–144.
Wiedenbeck, M., Alle, P., Corfu, F., Griffin, W.L., Meier, M., Oberli, F., Quadt, A.V., Roddick, J.C., Spiegel, W., 1995. Three natural zircon standards for U–Th–Pb, Lu–Hf, trace element and REE analyses. Geostandards and Geoanalytical Research 19, 1–23.

Wiedenbeck, M., Hanchar, J.M., Peck, W.H., Sylvester, P., Valley, J., Whitehouse, M., Kronz, A., Morishita, Y., Nasdala, L., Fiebig, J., Franchi, I., Girard, J.P., Greenwood, R.C., Hinton, R., Kita, N., Mason, P.R.D., Norman, M., Ogasawara, M., Piccoli, R., Rhede, D., Satoh, H., Schulz-Dobrick, B., Skar, O., Spicuzza, M.J., Terada, K., Tindle, A., Togashi, S., Vennemann, T., Xie, Q., Zheng, Y.F., 2004. Further characterisation of the 91500 zircon crystal. Geostandards and Geoanalytical Research 28, 9–39.

Woodhead, J., Hergt, J., Shelley, M., Eggins, S., Kemp, R., 2004. Zircon Hf-isotope analysis with an excimer laser, depth profiling, ablation of complex geometries, and concomitant age estimation. Chemical Geology 20, 121–135.

Wu, R.X., Zheng, Y.F., Wu, Y.B., Zhao, Z.F., Zhang, S.B., Liu, X.M., Wu, F.Y., 2006. Reworking of juvenile crust: element and isotope evidence from Neoproterozoic granodioritic in South China. Precambrian Research 146, 179–212.

Xu, Y.T., Shang, S.C., Zhang, B.H., 2000. Evidence for metallogenic geochemistry of volcano-hot spring deposition in Xiqiu copper massive sulfide deposit, Zhejiang province. Geochimica 29, 14–20 (in Chinese with English abstract).

Xu, J.F., Shinjo, R., Defant, M.J., Wang, Q., Rapp, R.P., 2002. Origin of Mesozoic adakitic intrusive rocks in the Ningzhen area of east China: partial melting of delaminated lower continental crust? Geology 30, 1111–1114.

Xu, P., Wu, F., Xie, L., Yang, Y., 2004. Hf isotopic compositions of the standard zircons for U–Pb dating. Chinese Science Bulletin 49, 1642–1648.

Yang, Z.M., Hou, Z.Q., 2009. Porphyry Cu deposits in collisional orogen setting: a preliminary genetic model. Mineral Deposits 28, 515–538 (in Chinese with English abstract).

Ye, M.F., 2006. SHRIMP U–Pb zircon geochronological, geochemical and Nd–Hf–O isotopic evidences for early Neoproterozoic Sibaoan magmatic arc along the southeastern margin of the Yangtze block. Master thesis, Graduate School of the Chinese Academy of Sciences. (in Chinese with English abstract).

Ye, M.F., Li, X.H., Li, W.X., Liu, Y., Li, Z.X., 2007. SHRIMP zircon U–Pb geochronological and whole-rock geochemical evidence for an early Neoproterozoic Sibaoan magmatic arc along the southeastern margin of the Yangtze Block. Gondwana Research 12, 144–156.

Zhang, Q., Wang, Y., Qian, Q., Yang, J.H., Wang, Y.L., Zhao, T.P., Guo, G.J., 2001. The characteristics and tectonic–metallogenic significances of the adakites in Yanshan period from eastern China. Acta Petrologica Sinica 17, 236–244 (in Chinese with English abstract).

Zhang, Q., Qin, K.Z., Wang, Y.L., Zhang, F.Q., Liu, H.T., Wang, Y., 2004. Study on adakite broadened to challenge the Cu and Au exploration in China. Acta Petrologica Sinica 20, 195–204 (in Chinese with English abstract).

Zhang, Q., Jin, W.J., Wang, Y.L., Li, C.D., Wang, Y., Jia, X.Q., 2006. A model of delamination of continental lower crust. Acta Petrologica Sinica 22, 265–276 (in Chinese with English abstract).

Zhang, Q., Wang, Y., Xiong, X.L., Li, C.D., 2008. Adakite and Granite: Challenge and Opportunity. China Land Press, Beijing, pp. 1–344 (in Chinese with English abstract).

Zheng, Y.F., Wu, Y.B., Chen, F.K., Gong, B., Li, L., Zhao, Z.F., 2004. Zircon U–Pb and oxygen isotope evidence for a large-scale ^{18}O depletion event in igneous rocks during the Neoproterozoic. Geochimica et Cosmochimica Acta 68, 4145–4165.

Zheng, Y.F., Wu, R.X., Wu, Y.B., Zhang, S.B., Yuan, H.L., Wu, F.Y., 2008. Rift melting of juvenile arc-derived crust: geochemical evidence from Neoproterozoic volcanic and granitic rocks in the Jiangnan Orogen, South China. Precambrian Research 163, 351–383.

Zhou, X.M., 1992. Magma mixing and their Precambrian basement along Jiang-Shao fault zone. Science in China Series B 3, 298–303 (in Chinese with English abstract).

Zhou, Q., Jiang, Y.H., Zhao, P., Liao, S.Y., Jin, G.D., 2011. Origin of the Dexing Cu-bearing porphyries, SE China: elemental and Sr–Nd–Pb–Hf isotopic constraints. International Geology Review, http://dx.doi.org/10.1080/00206814.2010.548119.

Zhu, X., Hang, C.K., Rui, Z.Y., Zhou, Y.H., Zhu, X.J., Hu, C.S., Mei, Z.K., 1983. The Geology of Dexing Porphyry Copper Ore Field. Geological Publishing House, Beijing, p. 336 (in Chinese with English abstract).

Zhu, J.C., Shen, W.Z., Liu, C.S., Xu, S.J., 1990. Nd–Sr characteristics and genetic discussion of Mesozoic granitoids of syntexis series in South China. Acta Petrologica et Mineralogica 9, 97–105 (in Chinese with English abstract).

Zhu, J.C., Jin, Z.D., Rao, B., Li, F.C., 2002. Ore-forming fluid process in the Dexing porphyry copper deposit, Jiangxi province: evidence from clay mineralogy, fluid inclusion and isotope tracing. Journal of Nanjing University (Natural Sciences) 38, 418–434 (in Chinese with English abstract).

Zuo, L.Y., Zhang, D.H., Li, J.K., Zhang, W.H., 2007. Source of ore-forming materials in the Dexing porphyry copper deposit, Jiangxi Province: evidence from aqueous fluid inclusions and silicate melt inclusions. Acta Geologica Sinica 81, 684–695 (in Chinese with English abstract).